POLITECNICO DI TORINO

Master's Degree in Aerospace Engineering

Master's Degree Thesis

Trajectory optimisation with Ant Colony Optimisation algorithm for multiple debris removal missions

Supervisor	Candidate
Prof. Lorenzo CASALINO	Giovanni Antonio STASI

December 2025

Summary

The intensification of space activity has led to a significant increase in orbital debris, posing a growing threat to the sustainability of orbital operations. With the expansion of satellite constellations, the phenomenon is set to worsen, making it essential to adopt Active Debris Removal (ADR) missions to mitigate collision risk and prevent the Kessler Syndrome, which could compromise entire orbital regions. The effectiveness of an ADR mission is closely related to the amount of debris removed in a single operation, a problem similar to the Travelling Salesman Problem (TSP). In this context, trajectory optimisation is addressed using an algorithm based on Ant Colony Optimisation (ACO), which emulates the stigmergy mechanisms observed in the cooperative behaviour of ants to identify optimal solutions to complex combinatorial problems.

Table of Contents

List of Tables

List of Figures

Acronyms

ACO
Ant Colony Optimisation

ADR
Active Debris Removal

EDT
Electro-Dynamic Tethers

ESA
European Space Agency

GEO
Geostationary Orbit

GNSS
Global Navigation Satellite System

GTOC9
Global Trajectory Optimisation Competition 9

JD
Julian Date

JPL
Jet Propulsion Laboratory

LEO
Low Earth Orbit

MJD2000

Modified Julian Date 2000

NASA

National Aeronautics and Space Administration

RAAN

Right Ascension of the Ascending Node

SRM

Solid Rocket Motors

SSO

Sun-Synchronous Orbit

TSP

Travelling Salesman Problem

US

United States

Chapter 1

Space debris

1.1 Introduction

Since the launch of Sputnik on 4 October 1957, humanity has continued to launch and put satellites into orbit, making them indispensable tools in our lives. From monitoring the environment and climate change to satellite navigation and telecommunications, space plays a fundamental role in our lives. As is often the case, human activity leaves its mark. In fact, after half a century of space activity, operational satellites account for only a fraction of the total number of objects orbiting Earth, with the remainder consisting of **space debris**. NASA's preferred terminology is **orbital debris**, which it defines as "all man-made objects in orbit about the Earth which no longer serve a useful purpose" [1]. Space debris occupies circumterrestrial orbits between 300 and 40,000 km in altitude, and the speed of debris ranges from a few kilometres per second to 10–15 km/s. Due to the increase in population density and the high relative orbital speeds involved, space debris poses a significant danger to operational satellites already in orbit, new satellites to be launched, and manned space missions, also considering the possible re-entry of some large debris into Earth's atmosphere [2]. For safety reasons, it is necessary to monitor debris. Still, only debris above a specific size can be tracked: large orbital debris (>10 cm) is routinely tracked by the U.S. Space Surveillance Network. Objects as small as 3 mm can be detected by ground-based radars, providing a basis for a statistical estimate of their numbers. Assessments of the population of orbital debris smaller than 1 mm can be made by examining impact features on the surfaces of returned spacecraft. However, this has been limited to spacecraft operating in altitudes below 600 km [1].

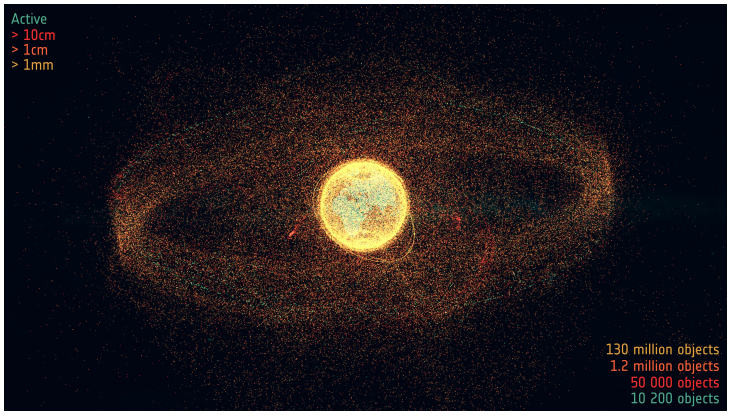

Figure 1.1: Space debris surrounding Earth [3]

Fundamental orbital mechanics predict (with rare exceptions) that any two orbiting objects that pass through the same distance from the objects that they are orbiting about represent an unstable condition. The condition is unstable because the two objects will eventually collide and break into several smaller fragments, creating an even larger number of objects at the same distance, thereby increasing the collision rate. In addition, as several investigations have concluded, atmospheric drag will not remove larger collision fragments faster than the current population of intact objects can generate them. Consequently, certain regions of low Earth orbit will likely see a slow but continuous increase in collision fragments, which will not stop until the intact population is reduced.

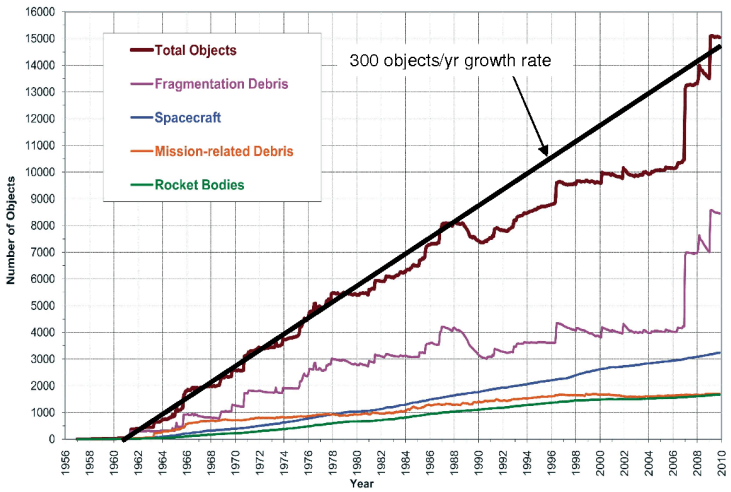

Figure 1.2: Growth of space debris [4]

The chain reaction of these collisions would cause certain orbits to become saturated,

making them unusable, a situation known as the **Kessler syndrome** [4].

1.2 Cause of the problem

Space debris is mainly formed in three ways: mission-related operations, accidents or intentional creation [5].

1.2.1 Mission-related operations

During the deployment phase of satellite operations, several items are deliberately released in orbit. These include [6]:

- spin-up devices or spring release mechanisms released when the spacecraft is separated from the launcher;
- debris from explosive bolts and pyrotechnic devices used for separating the spacecraft from the launch vehicle stages;
- large structural elements (dispensers) left in orbit in the event of a multiple launch;
- attach mechanisms released during deployment of antennas, solar panels, and other appendages;
- protective covers released during activation of optical, attitude, and other sensor systems.

Even the upper stages of launchers become debris, and in the case of solid launchers, in the final stages of combustion, aluminium oxide (Al_2O_3) particles measuring centimetres are released, contributing to the debris problem [7].

1.2.2 Accidental

Most "accidental" debris results from explosions or collisions between decommissioned or still-functioning satellites. Liquid-fuel rocket stages left in orbit with fuel remaining in their tanks have exploded between a few months and a few years after launch. Exposure to sunlight and temperature fluctuations can weaken their structure to the point of failure [5]. The first collision between satellites occurred on 10 February 2009 between the still-operational US satellite Iridium 33 and the decommissioned Russian satellite Kosmos 2251.
Of course, not all collisions generate the same effects. For the purpose of classifying collisions by the amount of debris generated, the consequences of collisions between catalogued objects can be divided into three types [4]:

1. **negligible non-catastrophic**: these collisions do not significantly affect either the long-term or short-term environment. This type of collision produces a negligible amount of debris;

2. **non-catastrophic**: these collisions contribute only to the short-term environment. In general, a non-catastrophic collision is one between a fragment and an intact object, and will generate an amount of debris that is about 100 times the mass of the impacting fragment;

3. **catastrophic**: this type of collision contributes both to the short-term and long-term environment. A catastrophic collision produces a small fragment population similar to that of a non-catastrophic collision, plus a population of larger fragments that significantly contribute to collisional cascading.

1.2.3 Intentional

On 11 January 2007, China conducted a test destroying the Fengyun 1C meteorological satellite. The test resulted in the creation of the most severe artificial debris cloud in Earth orbit since the beginning of space exploration. More than 2,000 debris items of 10cm or larger have been identified by the US Space Surveillance Network, representing an immediate increase of more than one-third in the catalogued Low Earth Orbit (LEO) debris environment. This population had accumulated over 50 years. The majority of the debris will remain in orbit for decades, some even lasting more than 100 years [8].

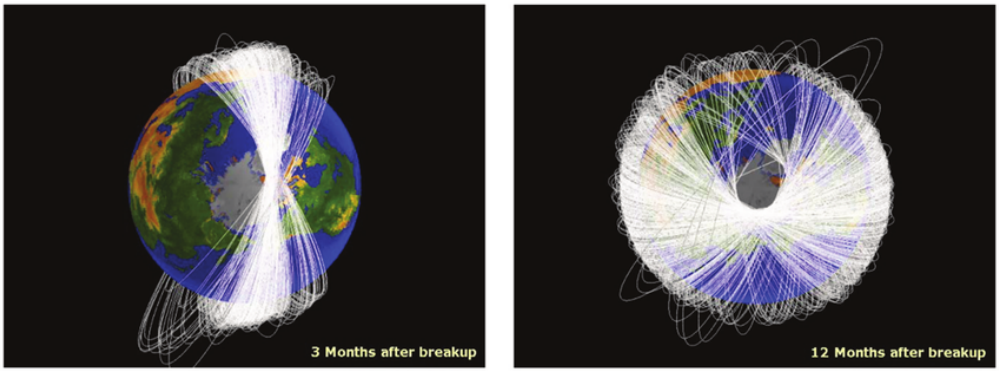

Figure 1.3: Debris distribution [8]

1.3 Up-to-date situation

Space traffic has been experiencing significant changes since 2015, especially in LEO, driven by the miniaturisation of space systems and the deployment of large

constellations, with a shift towards commercial operators [9]. The growth is mainly due to the new low-latency satellite internet business, which involves thousands of satellites in LEO to ensure global coverage. Companies like SpaceX, with its Starlink constellation, aim to place thousands of satellites in orbit, potentially worsening the already problematic issue of space debris and also impacting astronomy. Thus, it is vital to establish and enforce clear policies focused on collision avoidance, debris reduction, and the timely deorbiting of non-operational satellites as the primary mitigation strategy.

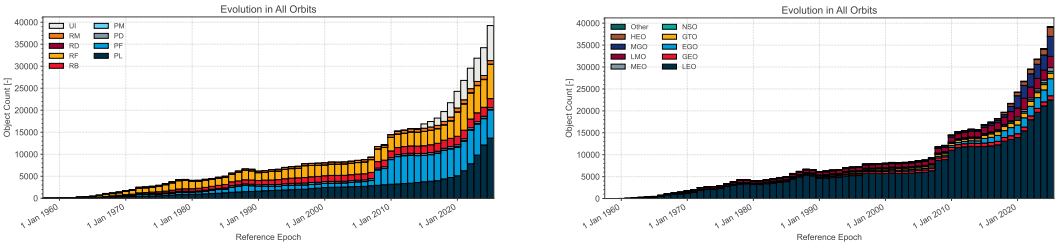

(a) Object class **(b)** Orbit class

Figure 1.4: Evolution of number of objects by object class and orbit class [9]

Type	Description
PL	Payload
PF	Payload Fragmentation Debris
PD	Payload Debris
PM	Payload Mission Related Object
RB	Rocket Body
RF	Rocket Fragmentation Debris
RD	Rocket Debris
RM	Rocket Mission Related Object
UI	Unidentified

Table 1.1: Object classifications [9]

Orbit	Description	Definition
LEO_{IADC}	IADC LEO Protected Region	$h \in [0,2000]$
GEO_{IADC}	IADC GEO Protected Region	$h \in [35586,35986] \quad \delta \in [-15,15]$

Table 1.2: Protected regions [9]

Orbit	Description	Definition		
GEO	Geostationary Orbit	$i \in [0,25]$	$h_p \in [35586,35986]$	$h_a \in [35586,35986]$
IGO	Inclined Geosynchronous Orbit	$a \in [37948,46380]$	$e \in [0.00,0.25]$	$i \in [25,180]$
EGO	Extended Geostationary Orbit	$a \in [37948,46380]$	$e \in [0.00,0.25]$	$i \in [0,25]$
NSO	Navigation Satellites Orbit	$i \in [50,70]$	$h_p \in [18100,24300]$	$h_a \in [18100,24300]$
GTO	GEO Transfer Orbit	$i \in [0,90]$	$h_p \in [0,2000]$	$h_a \in [31570,40002]$
MEO	Medium Earth Orbit	$h_p \in [2000,31570]$	$h_a \in [2000,31570]$	
GHO	GEO-superGEO Crossing Orbits	$h_p \in [31570,40002]$	$h_a > 40002$	
LEO	Low Earth Orbit	$h_p \in [0,2000]$	$h_a \in [0,2000]$	
HAO	High Altitude Earth Orbit	$h_p > 40002$	$h_a > 40002$	
MGO	MEO-GEO Crossing Orbits	$h_p \in [2000,31570]$	$h_a \in [31570,40002]$	
HEO	Highly Eccentric Earth Orbit	$h_p \in [0,31570]$	$h_a > 40002$	
LMO	LEO-MEO Crossing Orbits	$h_p \in [0,2000]$	$h_a \in [2000,31570]$	
UFO	Undefined Orbit			
ESO	Escape Orbits			

Table 1.3: Orbital classification (units in km and degrees) [9]

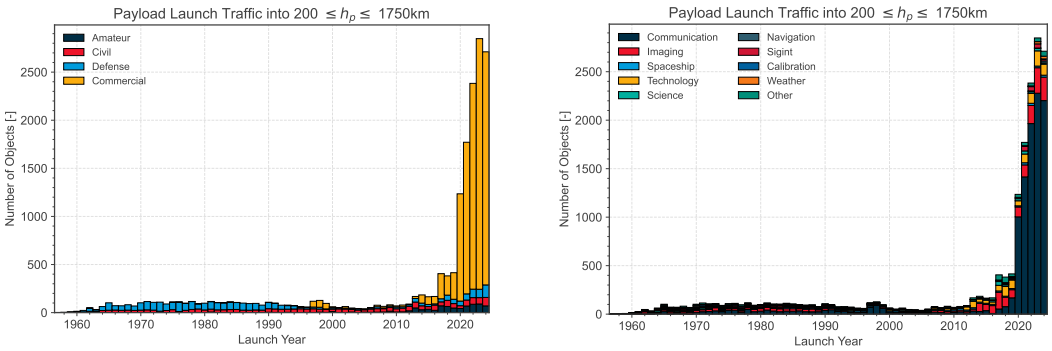

(a) Mission funding

(b) Type

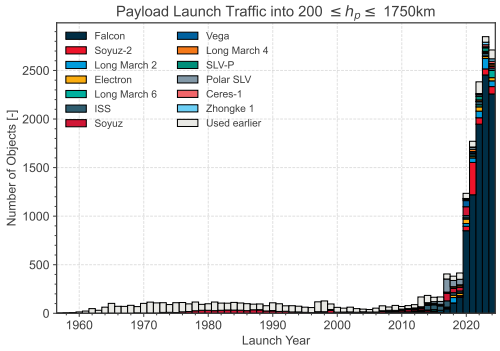

(c) Launcher family

Figure 1.5: Evolution of the launch traffic near LEO_{IADC} per mission funding, type and launcher family [9]

1.3.1 Debris characterization

Objects in the space environment can be categorised in two broad categories: those that can be traced back to a launch event and for which the nature can be identified, and those for which this is impossible. The latter ones will be identified as Unidentified, whereas the former can be further categorised in [9]:

- **payloads**: space object designed to perform a specific function in space, excluding launch functionality. This includes operational satellites as well as calibration objects;
- **payload mission related objects**: space objects released as space debris which served a purpose for the functioning of a payload. Common examples include covers for optical instruments or astronaut tools;
- **payload fragmentation debris**: space objects fragmented or unintentionally released from a payload as space debris for which their genesis can be traced back to a unique event. This class includes objects created when a payload explodes or when it collides with another object;
- **payload debris**: space objects fragmented or unintentionally released from a payload as space debris for which the genesis is unclear, but orbital or physical properties enable a correlation with a source;
- **rocket body**: space object designed to perform launch-related functionality; This includes the various orbital stages of launch vehicles, but not payloads, which release smaller payloads themselves;
- **rocket mission related objects**: space objects intentionally released as space debris which served a purpose for the function of a rocket body. Common examples include shrouds and engines;
- **rocket fragmentation debris**: space objects fragmented or unintentionally released from a rocket body as space debris for which their genesis can be traced back to a unique event. This class includes objects created when a launch vehicle explodes;
- **rocket debris**: space objects fragmented or unintentionally released from a rocket body as space debris for which the genesis is unclear, but orbital or physical properties enable a correlation with a source.

Another classification can be made based on the distance at which a satellite/debris orbits [10]:

- up to 500 km, the re-entry time into the atmosphere is less than 25 years;

- up to 800 km, the re-entry time is 100-150 years;
- up to 1200 km, the re-entry time is approximately 2000 years;
- in Geostationary Orbit (GEO), approximately 36000 km, we are talking about millions of years.

For this reason, especially in orbits above 500 km, de-orbiting manoeuvres must be implemented. In a GEO, it is preferable to move the satellite into a graveyard orbit.

1.4 Potential solutions

1.4.1 New requirements

Concerns about the growing amount of orbital debris have led organisations such as the ESA to implement strategies to mitigate their presence. The main features of the ESA's Zero Debris approach are listed below [11]:

1. **guarantee successful disposal**: self-disposal through atmospheric reentry or re-orbiting to a safe altitude should be verified in advance of a mission's launch, with a probability of success higher than 90%. Critical disposal functions (such as enough fuel for manoeuvres, functioning thrusters, etc) should be continuously monitored. Missions should also include interfaces that would facilitate removal from orbit if self-disposal fails;
2. **improve orbital clearance**: by reducing the time an object is in orbit, the smaller the chance that it will collide with another object and create further debris. ESA's Zero Debris recommendations propose that a satellite or rocket body in LEO should not remain in orbit longer than 5 years after its end of life, and require that the cumulative probability of collision with any debris larger than 1 cm in size is below 1 in 1000 for the entire period of a mission's life, until it re-enters Earth's atmosphere;
3. **avoid in-orbit collisions**: it comes at a cost as fuel is required and instruments are often turned off, meaning data is lost. With the dramatic rise in space activity and the growth in orbital debris, the number of collision alerts received each week and the manoeuvres required are also increasing. Improved collision avoidance strategies, using automation, traffic coordination, communication protocols and more, are needed as the risk of collision increases;
4. **avoid internal break-ups**: enhanced health monitoring and robust passivation techniques should be implemented to prevent satellites breaking up from

within, caused by system explosions from leftover fuel or energy from solar panels;

5. **prevent intentional release of space debris**: the deliberate release of any "Mission Related Object" (such as protective covers, lens caps, rocket fairings) should be avoided to prevent further debris growth;

6. **improve on-ground casualty risk assessment**: standardised tools and methodologies should be developed for assessing the casualty risk, on the ground, of re-entering objects, as well as for verifying evaluations of how a mission will end;

7. **guarantee Dark and Quiet skies**: measures should be identified and implemented to minimise the impact of space objects on optical and infrared astronomy, as well as radio astronomy, to maintain dark and quiet skies;

8. **beyond the protected regions** (see Table 1.2): other orbits, such as those used by Global Navigation Satellite System (GNSS) constellations and lunar orbits, should also be considered and protected to ensure their long-term sustainability. Adapted Zero Debris recommendations should be formulated and applied beyond LEO and GEO.

1.4.2 Active Debris Removal

Projections showing the use of Active Debris Removal (ADR) technology demonstrate that if three to five pieces of the most concerning debris objects were removed per year, this environment could be stabilised, and that the removal of ten or more per year would begin the process of mitigating the problem [12]:

- **Electro-Dynamic Tethers** (EDT): this method exploits the interaction between a conductive tether and the Earth's magnetic field. The debris object is linked to a de-orbiting element via a conductive tether, with both ends electrically connected to the ionospheric plasma. As the tether moves through the magnetic field at orbital velocity, an electric current is induced, generating a Lorentz force that decelerates the attached object and accelerates its orbital decay. The technological constraints include potential difficulties in securing the tether, which could be addressed using a harpoon, a hooked net, or an adhesive suction cup. The use of tethers also increases the cross-sectional area and, consequently, the likelihood of conjunction collisions with other objects, although to a lesser extent than with other proposed methods.

- **Capture and Removal**: this is another promising technique, and various initiatives have been undertaken to study these scenarios. In essence, this

approach involves capturing an arbitrarily rotating object using robotic arms or other mechanisms. Once captured, the object is transferred by the ADR vehicle to a new disposal orbit through a velocity impulse. This technique is not particularly useful in LEO, but it is the preferred disposal method in GEO, where satellites, rocket stages, and similar objects are moved to a higher parking or graveyard orbit.

- **Momentum Exchange Tethers**: typically, a vehicle in a higher orbit attaches a tether to one in a lower orbit. The difference in velocity and perturbing accelerations causes both vehicles to swing along an arc defined by the tether. If the lower object is released at the point of greatest retrograde velocity, its perigee will be lowered while the apogee of the higher object will be raised. Conceptually, momentum exchange tethers appear promising for ADR activities; however, theoretical analyses indicate that a 10 km tether would be required to lower an orbit by just 100 km. These requirements differ significantly from those of tethers used in EDT methods and may render momentum exchange tethers impractical due to the increased collision risk associated with their large size.

- **Lasers**: the use of lasers for ADR is highly questionable. Maintaining a tightly focused beam on a rapidly and unpredictably moving target for a prolonged period, sufficient to ablate its surface and induce acceleration, is technically challenging. The deployment of such lasers would also raise concerns regarding compliance with international weapons treaties and United Nations regulations. In addition, many debris objects may contain unspent propellant that could explode if heated by a laser, creating even more debris.

- **Surface Material**: the basic concept involves deploying a large, thin surface that causes objects striking it to experience a change in momentum, thereby slowing them down and lowering their orbits. An alternative approach would be to release a low-density material that captures or decelerates debris as it passes through. However, such materials carry the risk of inducing fragmentation events, and the level of deceleration achievable with a material thin enough to avoid this risk is minimal.

- **Solar Sails**: a thin reflective material is deployed from an orbiting body, and solar photons striking the surface are reflected, imparting a slight acceleration to the object. Solar sails are more effective for orbital modifications that do not involve a net energy exchange and are therefore particularly suitable for altering orbital eccentricity. In practice, the main contribution to altitude reduction or de-orbiting comes from increased atmospheric drag rather than the photon pressure itself. However, this effect becomes largely ineffective below 800 km altitude due to the corrosive nature of the ionosphere on the

sail material. Furthermore, achieving an acceleration sufficient to produce a noticeable orbital change may take several months. In the meantime, the attached solar sail significantly increases the object's cross-sectional area, thereby raising the risk of collision or interference with other orbiting bodies.

- **Solid Rocket Motors** (SRM): the basic concept involves launching an ADR vehicle equipped with multiple small propulsion stages that can be deployed and attached to large debris objects. However, this technique presents several challenges, including increased launch mass due to the required SRM casing and propellant, as well as the difficulty of attaching an SRM to an arbitrarily rotating and unprepared surface. Even if an SRM could be successfully connected, the module would require a complex attitude determination system to ensure that the motor is fired at the right moment, so that the resulting change in velocity effectively lowers the orbit of the target debris object.

1.4.3 Environmental issue

The problem of space debris is far from being solved, and another issue immediately arises: the increase in satellite numbers and the de-orbiting of debris into the atmosphere lead to the dispersion of pollutants, posing serious environmental problems.

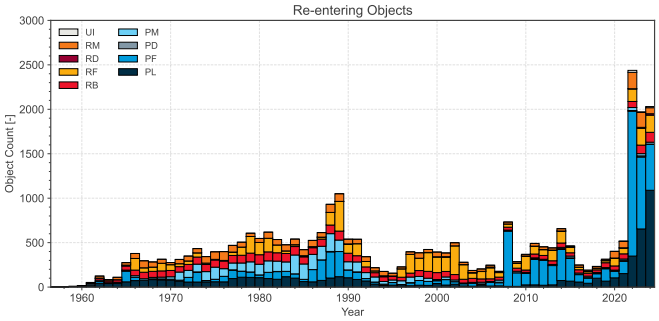

Figure 1.6: Re-entering objects [9]

Satellites disintegrate during atmospheric reentry at the conclusion of their operational lifespan, experiencing a loss of between 51% and 95% of their mass. Aluminium, a fundamental structural material in spacecraft and launch vehicles, interacts with oxygen in this process to produce aluminium oxides. These oxides are recognised as catalysts for chlorine activation reactions, which contribute to the depletion of stratospheric ozone, with an estimated reaction probability of approximately 2%. For a standard 250-kg satellite with a 30% aluminium mass fraction, roughly 32% of the aluminium is oxidised, resulting in approximately

30 kilograms of aluminium oxide nanoparticles. These particles can remain in the atmosphere for several decades, gradually descending from the mesosphere to the stratosphere over about 30 years. Upon reaching altitudes near 40 km, they enhance chlorine activation, thereby contributing to ozone depletion. This prolonged residence time implies that the effects of ozone depletion are delayed in relation to the timing of satellite reentries. In 2022, the total aluminium re-entering from satellites was estimated at 41.7 metric tons, approximately 29.5% above the natural aluminium influx from micrometeoroids, resulting in approximately 16–17 metric tons of aluminium oxide. Modelling studies suggest that nitrogen oxides and chlorine are also produced during reentry, with long-term ozone depletion expected primarily over Antarctica at high altitudes. Forecasts involving mega-constellations indicate that the reentry of numerous satellites could release over 360 metric tons of aluminium oxide compounds annually, which is more than 640% above natural levels and may lead to notable ozone depletion [13].

Chapter 2

Astrodynamics

Orbital mechanics and astrodynamics focus on the motion of celestial bodies and artificial satellites.

2.1 Two body problem

The two-body problem is based on two of Newton's laws: Newton's second law and the law of universal gravitation. Although the two-body problem is a simplification of the n-body problem, it can describe phenomena such as the motion of the Earth around the Sun or, as in this thesis, the motion of satellites/space debris around the Earth quite well. The simplifications compared to the n-body problem are:

- the problem is characterised only by two masses with spherical symmetry and M > m;
- the only force acting on the system is the gravitational force;
- the problem is studied in an inertial reference plane.

Let (X', Y', Z') be an inertial set of rectangular Cartesian coordinates. Let (X, Y, Z) be a set of non-rotating coordinates parallel to (X', Y', Z') and having an origin coincident with the body of mass M. The position vectors of the bodies M and m with respect to the set (X', Y', Z') are r_M and r_m respectively, defining vector $\mathbf{r}$ as [14]:

$$\mathbf{r} = \mathbf{r_m} - \mathbf{r_M} \tag{2.1}$$

The same thing can be done with the acceleration vector:

$$\ddot{\mathbf{r}} = \ddot{\mathbf{r}}_\mathbf{m} - \ddot{\mathbf{r}}_\mathbf{M} \tag{2.2}$$

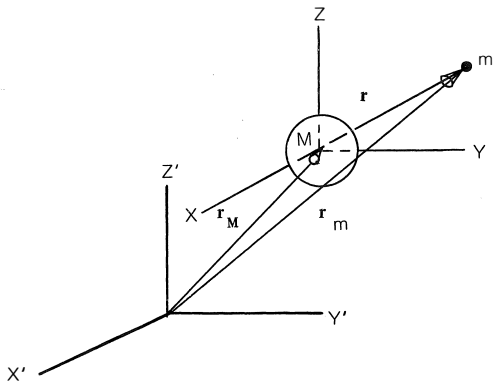

Figure 2.1: Relative motion of two bodies [14]

Applying Newton's laws, with G = $6.673 \cdot 10^{-11} \frac{m^3}{kg\ s^2}$, we obtain:

$$m\ddot{\mathbf{r}}_{\mathbf{m}} = -\frac{GMm}{r^2}\frac{\mathbf{r}}{r} \tag{2.3}$$

$$M\ddot{\mathbf{r}}_{\mathbf{M}} = \frac{GMm}{r^2}\frac{\mathbf{r}}{r} \tag{2.4}$$

Simplifying m in the first equation and M in the second, and subtracting the second equation from the first, we obtain:

$$\ddot{\mathbf{r}} = -\frac{G(M+m)}{r^3}\mathbf{r} \tag{2.5}$$

In the case study, since we are dealing with space debris orbiting Earth, $M >> m$, therefore $G(M+m) \approx GM \equiv \mu$. μ is called the gravitational parameter (in this case, Earth's gravitational parameter). Substituting into the Equation 2.5, we obtain the equation for the two-body problem:

$$\ddot{\mathbf{r}} + \frac{\mu}{r^3}\mathbf{r} = 0 \tag{2.6}$$

2.1.1 Constant of motion

Two quantities of particular importance in describing the motion of a body around a central body are **specific mechanical energy ϵ** and **specific angular momentum h**. Since Newtonian gravity is a central force, i.e. directed along the line connecting the two bodies and dependent solely on their mutual distance, it is possible to study their conservation.

Specific mechanical energy ϵ

Starting from Equation 2.6, we dot-multiply both terms by the velocity vector $\dot{\mathbf{r}}$ and then, rearranging the products and the terms, we obtain:

$$v\dot{v} + \frac{\mu}{r^2}\dot{r} = 0 \tag{2.7}$$

The first term is the derivative of the specific kinetic energy, while the second one is the derivative of the specific potential energy:

$$\frac{d}{dt}\left(\frac{v^2}{2}\right) + \frac{d}{dt}\left(-\frac{\mu}{r}\right) = 0 \quad \Rightarrow \quad \frac{d}{dt}\left(\frac{v^2}{2} - \frac{\mu}{r}\right) = 0 \tag{2.8}$$

If the time rate of change of an expression is zero, that expression must be a constant. Integrating both sides of the equation with respect to time, we obtain the **vis-viva** equation:

$$\epsilon = \frac{v^2}{2} + c - \frac{\mu}{r} \tag{2.9}$$

The choice of c is arbitrary and, in orbital mechanics, c is set equal to zero, i.e. the zero potential energy is set to infinity. The downside is that a satellite's potential energy will always be negative.
Finally, we get to the final equation for specific mechanical energy, which can also be traced back entirely to the semi-major axis a (see Section 2.1.2) of the orbit:

$$\epsilon = \frac{v^2}{2} - \frac{\mu}{r} = -\frac{\mu}{2a} \tag{2.10}$$

The specific mechanical energy is constant along the orbit.

Specific angular momentum h

Starting again from Equation 2.6, this cross-multiplying by vector $\mathbf{r}$. We obtain:

$$\mathbf{r} \times \ddot{\mathbf{r}} + \mathbf{r} \times \frac{\mu}{r^3}\mathbf{r} = 0 \tag{2.11}$$

The second term is equal to zero, and the first term is rearranged considering the following differential:

$$\frac{d}{dt}(\mathbf{r} \times \dot{\mathbf{r}}) = \dot{\mathbf{r}} \times \dot{\mathbf{r}} + \mathbf{r} \times \ddot{\mathbf{r}} = 0 \quad \Rightarrow \quad \frac{d}{dt}(\mathbf{r} \times \mathbf{v}) = 0 \quad \Rightarrow \quad \mathbf{h} = \mathbf{r} \times \mathbf{v} \tag{2.12}$$

We have shown that the specific angular momentum is constant and perpendicular to the plane on which the position vector $\mathbf{r}$ and the velocity vector $\mathbf{v}$ lie, i.e. the **orbital plane**.

2.1.2 Orbits and orbital parameters

Integrating Equation 2.6 gives the equation of the trajectory written in polar coordinates, which also represents the equation of a conic section in polar coordinates:

$$r = \frac{\frac{h^2}{\mu}}{1 + \frac{B}{\mu}\, cos\nu} = \frac{p}{1 + e\ cos\nu} \tag{2.13}$$

The similarities between the equation of the trajectory and that of the conic section, in addition to verifying Kepler's First Law, allow us to make further considerations on the motion of a satellite in the two-body problem (some of which have already been anticipated) [14]:

1. the family of curves called **conic sections** (circle, ellipse, parabola, hyperbola) represents the only possible paths for an orbiting object in the two-body problem. The ellipse and the circle are closed orbits (of our interest) while the parabola and the hyperbola are open orbits (see Table 2.1);
2. the focus of the conic orbit must be located at the centre of the central body;
3. the mechanical energy of a satellite (the sum of its kinetic and potential energy) does not change as the satellite moves along its conic orbit. There is, however, an exchange of energy between the two forms, potential and kinetic, which means that the satellite must slow down as it gains altitude (as r increases) and speed up as r decreases in such a manner that ϵ remains constant;
4. the orbital motion takes place in a plane which is fixed in inertial space;
5. the specific angular momentum of a satellite about the central attracting body remains constant.

Mechanical Energy	**Semi-major axis**	**Eccentricity**	**Conic**
$\varepsilon < 0$	$a > 0$	$e = 0$	Circumference
$\varepsilon < 0$	$a > 0$	$0 < \mathrm{e} < 1$	Ellipse
$\varepsilon = 0$	$a \to \infty$	$\mathrm{e} = 1$	Parabola
$\varepsilon > 0$	$a < 0$	$\mathrm{e} > 1$	Hyperbole

Table 2.1: Conics classifications

To describe an orbit, firstly, we need an inertial reference plane. For a satellite orbiting the Earth, we use the geocentric-equatorial system (**IJK**). It originates at the centre of the Earth, and the fundamental plane is the equatorial plane. The

X-axis points in the direction of the vernal equinox, the Z-axis towards the North Pole, and the Y-axis in such a way as to comply with the right-hand rule. This system does not rotate with the Earth but is fixed relative to the fixed stars (except for precession phenomena).

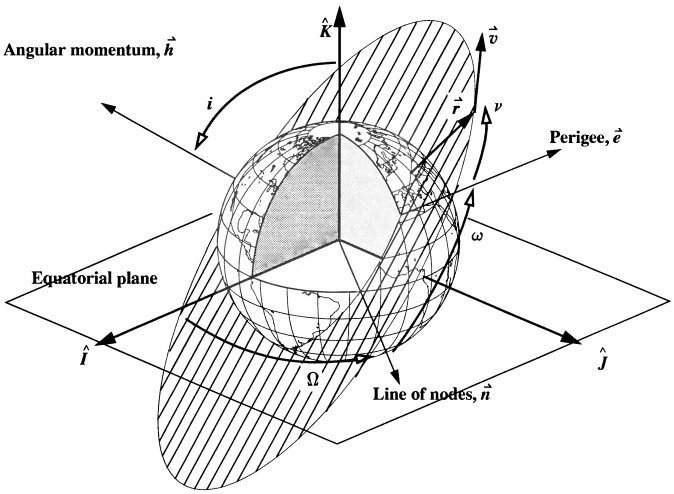

Figure 2.2: Orbital elements [15]

We define six parameters, known as **classical orbital elements**: five to describe the size, shape, and orientation of the orbit, and one to determine the satellite's location in a given moment:

- **a**, **semi-major axis**: half of the major axis, defining the size of the orbit;
- **e**, **eccentricity**: magnitude of the vector **e** pointing to periapsis, defining the shape of the orbit;
- **i**, **inclination**: angle of tilt of the orbital plane with respect to Earth's equatorial plane. It is measured between **K** and vector **h**;
- **Ω**, **Right Ascension of the Ascending Node (RAAN)**: angle on the Earth's equatorial plane measured counterclockwise from **I** to the ascending node, i.e. the point in the orbit where the satellite crosses the equatorial plane moving northwards (conversely, at the descending node it crosses it moving southwards). The two nodes lie on the line of nodes, with vector **n** pointing towards the ascending node. The RAAN represents the longitude of the ascending node;

- $\boldsymbol{\omega}$, **argument of periapsis**: angle indicating the position of the periapsis in the orbit. It is measured in the orbital plane, starting from the ascending node;
- $\boldsymbol{\nu}$, **true anomaly**: angle in the orbital plane between the periapsis and the position of the satellite at a particular time, called epoch.

Another characteristic element of an orbit is the **semi-latus rectum p**, half the length of the latus rectum, which is the chord of a section passing through the focus and parallel to the directrix. Finally, the **apoastrum** and **periastrum** are defined as the furthest and nearest points to the central body.

2.2 Orbital perturbations

The actual trajectory of an artificial satellite differs from the ideal two-body Keplerian path as a result of perturbations caused by the gravitational influence of other celestial bodies (such as the Moon and the Sun) and by additional forces not accounted for in the Keplerian framework, including those arising from the nonspherical nature of the Earth. Neglecting Earth's oblateness leads to substantial inaccuracies in the long-term prediction of a satellite's position. A **perturbation** is defined as any force that induces a deviation from ideal Keplerian motion. Consequently, the propagation of a real orbit cannot be performed accurately using the restricted two-body theory. While actual orbits may closely approximate Keplerian motion over short time intervals, they invariably diverge from it due to the influence of these perturbative forces.
Orbital perturbations may be classified according to several criteria:

1. By **physical origin**:
    - **gravitational perturbations**: from third-body interactions (primarily the Moon and the Sun) and from the Earth's nonspherical mass distribution;
    - **non-gravitational perturbations**: including atmospheric drag, solar radiation pressure, and tidal friction.
2. By **energy characteristics**:
    - **conservative forces**: depend solely on position;
    - **non-conservative forces**: depend on both position and velocity.
3. By their **effect on the Keplerian orbital elements**:

- **secular variations**: corresponding to linear changes in the orbital elements over time;
- **long-period variations**: exhibiting oscillations with periods greater than the orbital period;
- **short-period variations**: exhibiting oscillations with periods shorter than the orbital period.

The most significant perturbations affecting Earth-orbiting satellites are:

- the non-spherical mass distribution of the Earth;
- third-body perturbations;
- atmospheric drag;
- solar radiation pressure.

The perturbation of most significant interest for this thesis, which will therefore be explored in depth, concerns the non-sphericity of the Earth.

2.2.1 Non-spherical Earth

The principal source of orbital perturbation for Earth satellites is the planet's non-sphericity and non-uniform mass distribution. The equipotential surfaces of the terrestrial gravitational field are not perfectly spherical but rather ellipsoidal, exhibiting regional irregularities. The **geoid** represents the idealised surface that, at every point, is perpendicular to the local direction of the gravity vector.
The Earth's gravitational potential can be expressed as a series expansion involving zonal, sectoral, and tesseral harmonic coefficients. Zonal coefficients J_n quantify the deviations of the gravitational field from spherical symmetry. Among these, the coefficient J_2 ($J_2 = 0.00108263$), representing the equatorial bulge, is the most significant, approximately one thousand times larger than the next coefficient J_3 ($J_1 = 0$). This term accounts for the dominant portion of the Earth's gravitational deviation from a perfect sphere.
The additional gravitational attraction caused by the equatorial bulge introduces a lateral force component directed toward the equatorial plane. This results in a torque acting on the satellite about the Earth's centre, inducing a precession of the orbital plane analogous to that of a gyroscope under an applied torque. The observable major consequences are a **regression of the line of nodes** and a **rotation of the line of apsides**, and also an effect on the mean anomaly M.

Nodal regression

The regression of the line of nodes consists of the rotation of the orbital plane around the Earth's rotational axis at a rate dependent on both orbital inclination and altitude. As a result, successive ground tracks of a direct (prograde) orbit are displaced westward relative to the displacement that would occur due to Earth's rotation alone [14]:

$$\frac{d\Omega}{dt} = \dot{\Omega} = -\frac{3}{2}\sqrt{\frac{\mu}{a^3}}\frac{J_2 \cos i}{(1-e^2)^2}\left(\frac{r_E}{a}\right)^2 \tag{2.14}$$

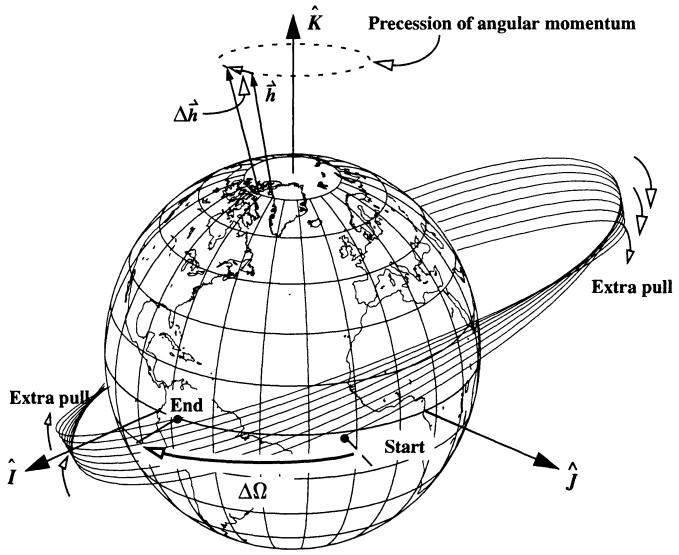

Figure 2.3: Nodal regression [15]

Apsidal rotation

The rotation of the line of apsides corresponds to a rotation of the major axis of the elliptical orbit. The direction of this rotation depends on the inclination: it occurs in the direction of motion (**precession**) for inclinations below 63.4° or above 116.6°, and opposite to the direction of motion (**regression**) for inclinations between these values. If the inclination is exactly 63.4° or 116.6°, the apsidal rotation induced by the J_2 term is nullified [14]:

$$\frac{d\omega}{dt} = \dot{\omega} = \frac{3}{4}\sqrt{\frac{\mu}{a^3}}\frac{J_2\left(5\cos^2 i - 1\right)}{(1-e^2)^2}\left(\frac{r_E}{a}\right)^2 \tag{2.15}$$

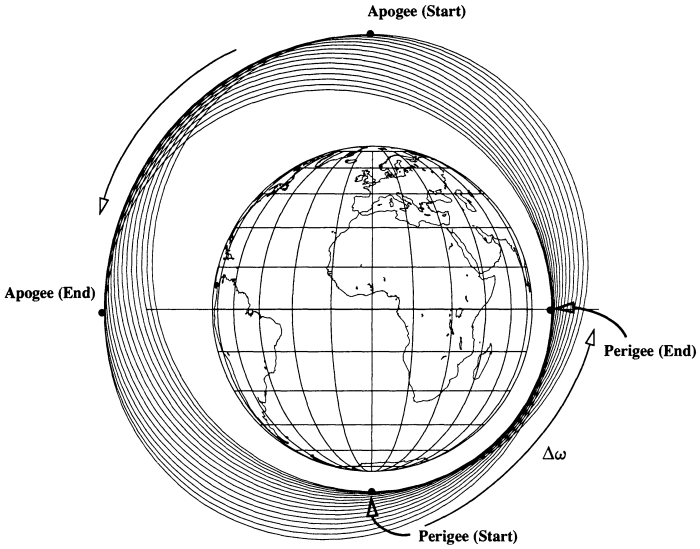

Figure 2.4: Apsidal rotation [15]

Mean anomaly

For an elliptical orbit, it is possible to define an auxiliary circle that circumscribes it. The **mean anomaly** is then defined as the angle that a satellite would sweep from periapsis if it were moving along this auxiliary circle at a constant angular rate, completing one revolution in the same period as the body on the actual elliptical orbit. Due to the effect of J_2, the mean anomaly changes as [14]:

$$\frac{dM}{dt} = \dot{M} = \sqrt{\frac{\mu}{a^3}} + \frac{3}{4}\sqrt{\frac{\mu}{a^3}}\frac{J_2\left(3\cos^2 i - 1\right)}{\left(1-e^2\right)^{3/2}}\left(\frac{r_E}{a}\right)^2 \tag{2.16}$$

2.2.2 Special orbits

The effect of J_2 is exploited to obtain orbits with specific effects, such as orbits **Sun-synchronous** orbit (SSO) and **Molniya** orbit.

Sun-synchronous orbit

A SSO is an orbit whose orbital plane precesses about the Earth's rotation axis at a rate that matches the mean apparent motion of the Sun, such that the satellite passes over any given ground point at approximately the same local mean solar time on each pass. This particular behaviour is achieved by designing the orbit so that the natural J_2-induced nodal regression rate equals the required solar precession rate ($\approx 360°$ per sidereal year, or $\approx 0.986°$ per day).

Molniya orbit

A Molniya orbit is a highly elliptical, high-inclination Earth orbit specifically designed to provide extended coverage of high-latitude regions, where geostationary satellites have limited visibility. It exploits the inclination of 63.4°, where the secular variation of the argument of perigee caused by the Earth's oblateness (the J_2 perturbation) is nullified, to stabilise the orientation of the orbit in space, minimising long-term rotation of the line of apsides and reducing the need for frequent station-keeping manoeuvres.

2.3 Orbital manoeuvres

In space, where there is a vacuum, the only way to modify the orbital elements of an orbit is to use Newton's principle of action-reaction by expelling gas from the spacecraft's engine. All fuel must be stored on board the spacecraft, so it is essential to calculate ΔV accurately, as this represents the cost of manoeuvring and must therefore be minimised. The ideal ΔV can be obtained using the rocket equation or Tsiolkovsky's equation:

$$\Delta V = c \ \ln \frac{m_i}{m_f} \tag{2.17}$$

ΔV can represent a change in the intensity or direction of the velocity vector, or both, and is related to the change in mass of the spacecraft. In Equation 2.17 m_i represents the initial mass, m_f the final mass and c the effective exhaust velocity. To obtain a more accurate value, it is necessary to account for aerodynamic, thrust misalignment, and gravity losses.
There are two types of orbital manoeuvres: impulsive and continuous. The impulsive manoeuvre fairly accurately describes chemical propulsion (the subject of this thesis), in which it is assumed that the thrust is applied so quickly that the spacecraft does not change its position in space.
Manoeuvres can essentially modify two aspects of an orbit: the orbit's energy and the orbital plane.
The former modifies the semi-major axis (see Equation 2.10) of the orbit by acting with thrust parallel to the velocity. The manoeuvre is more efficient at low radii because the orbital velocity is greater, achieving greater energy variations with the same ΔV:

$$dE = V dV \tag{2.18}$$

The second type of manoeuvre generally modifies both i and Ω and, unlike the first, is more efficient at high radii as it is possible to obtain the same $\Delta\psi$ (ψ is the azimuth angle) with a lower ΔV:

$$\Delta V = 2V \sin \frac{\Delta \psi}{2} \tag{2.19}$$

2.4 Time measure

Time represents a fundamental dimension in virtually all branches of science. In the field of astrodynamics, its importance is particularly pronounced, since celestial objects travel vast distances at high velocities. For a time system to be practical and reliable, it must be based on a precise and reproducible time interval defined by a measurable physical phenomenon. Furthermore, it is essential to establish a reference epoch from which all time intervals are consistently measured and expressed [15].
The **Julian Date** (JD) represents the continuous count of days elapsed since noon on Monday, 1 January 4713 BC (Julian calendar). The JD system was developed to provide astronomers with a uniform, continuous time scale that bridges different calendar systems and historical chronologies, offering a consistent temporal reference for astronomical computations. The JD system is based on the Julian Period, introduced by Joseph Scaliger in 1583. This period results from the product of three distinct calendar cycles:

$$15\ (Indiction\ cycle) \times 19\ (Metonic\ cycle) \times 28\ (Solar\ cycle)\ =\ 7980\ years$$

Its epoch (starting point) is set at the last time all three cycles were together in their first year. Because the JD system starts so far in the past, the corresponding day numbers can become huge to handle. To simplify calculations and data storage, especially in early computer systems with limited memory, a more recent reference epoch is sometimes adopted by omitting the most significant digits of the JD. An example of this simplification is the **Modified Julian Date 2000** (MJD2000), introduced by the ESA. It is defined in terms of the JD as:

$$MJD2000 = JD - 2451544.5$$

The subtraction of 0.5 is meant to match the start of the count with midnight of January 1, 2000, rather than midday [16].

Chapter 3

Problem description

The problem analysed in this thesis is based on the set of 123 debris from the Global Trajectory Optimisation Competition 9 (GTOC9) [17], an international competition created by Dario Izzo of the Advanced Concepts Team of the ESA. The following chapter will introduce the problem addressed, the winning solution from NASA's Jet Propulsion Laboratory (JPL) [18], and the differences between the problem addressed in the thesis and the original formulation.

3.1 GTOC 9

The competition is based on creating an ADR mission to make a SSO reusable after an explosion that generated a scenario similar to the Kessler syndrome (see Section 1.1). The resulting task is a global optimisation problem characterised by many local minima. Specific formulations of this trajectory design problem can be mapped onto complex variants of the Travelling Salesman Problem (TSP), placing them within the class of $\mathcal{NP}$-hard problems (see Section 4.1). Planning long debris-removal sequences is particularly demanding because the differential J_2 perturbation causes the RAAN values to evolve into a highly non-uniform and time-dependent distribution. The objective is to design n missions capable of removing a total of $M = 123$ debris objects, each orbiting along a Keplerian trajectory perturbed by the mean J_2 effect. Each mission consists of a multiple-rendezvous spacecraft trajectory, in which a subset of N out of the M debris items is targeted. The spacecraft delivers and activates N de-orbit packages, one for each selected object. Between successive rendezvous, the spacecraft follows Keplerian motion influenced by the full J_2 perturbation.

The mission design problem involves minimising the following cost function:

$$J = \sum_{i=1}^{n} C_i = \sum_{i=1}^{n} \left[c_i + \alpha \left(m_{0_i} - m_{dry} \right)^2 \right] \tag{3.1}$$

The total cost for the i-th mission C_i, as charged by the contracted launcher supplier, is determined by two primary components: the first is a base cost c_i, the value of which increases linearly throughout the competition time frame; the second is a term that incentivises a lighter spacecraft $\alpha(m_{0i} - m_{\text{dry}})^2$. In this formulation, m_{0i} is the total mass of the spacecraft at the beginning of the i-th mission and m_{dry} is the spacecraft's dry mass. Therefore, saving each kilogram of launch mass results in a discount applied to the overall mission cost. The basic cost c_i of each mission increases linearly during the month of the competition and is calculated as follows:

$$c_i = c_m + \frac{t_{\text{submission}} - t_{\text{start}}}{t_{\text{end}} - t_{\text{start}}} \left(c_M - c_m \right) \tag{3.2}$$

In this formulation, $t_{submission}$ denotes the epoch at which the i-th mission is submitted for validation, while t_{start} and t_{end} represent the start and end times of the GTOC9 competition window. The baseline mission cost c_m is set to 45 MEUR, whereas the upper bound c_M is 55 MEUR. Any debris object that is not removed by any of the planned missions is assumed to be cleared at the end of the competition by means of an individual launch, which carries a fixed penalty cost of $c_{penalty} = 55.0018$ MEUR.
The initial mass m_0 of each spacecraft is given by the sum of its dry mass, the combined mass of the $N \geq 1$ de-orbit packages it will deploy, and the propellant mass, that is:

$$m_0 = m_{dry} + N m_{de} + m_p \tag{3.3}$$

All spacecraft are assumed to have a dry mass of $m_{dry} = 2000$ kg and can carry at most $m_p = 5000$ kg of propellant, although using less propellant is possible and would reduce launch costs. Each de-orbit package has a constant mass of $m_{de} = 30$ kg.
Finally, there are some constraints to adhere to:

1. the i-th mission starts at epoch t_i^s and ends at epoch t_i^f. A mission begins with the insertion of the spacecraft at a selected debris and terminates once all N de-orbit packages have been deployed;

2. a debris is considered removed if its position and velocity vectors match those of the spacecraft at some epoch t, and the spacecraft remains nearby for $t_w = 5$ days to deliver and activate the de-orbit package;

3. only during the transfers between debris targets is the spacecraft subjected to the full J_2 perturbation;

4. the time interval between two consecutive debris rendezvous within the same mission must not exceed 30 days. Therefore, if the arrival epoch at debris a is t_a and the arrival epoch at the subsequent debris b is t_b, the following condition must hold: $t_b - t_a \leq t_R = 30$ days;

5. different missions cannot be operated in parallel. Moreover, a minimum time interval of $t_M = 30$ days must separate any two consecutive missions. Therefore, for all $i = j$, the following condition must be satisfied: $t_j^f + 30 \leq t_i^s$ [days] if $t_i^s > t_j^s$, where t_i^s and t_j^f denote the start epoch of mission i and the end epoch of mission j, respectively;

6. all mission events must occur within a prescribed time window. Therefore, for every event taking place at epoch t_{event}, the following condition must hold: $23467 \leq t_{\text{event}} \leq 26419$ (MJD2000), which corresponds to an 8 year interval;

7. the osculating orbital periapsis r_p must remain above the minimum allowed value, $r_{p,\min} = 6600000$ m. For simplicity, this constraint is verified only immediately after arrival, at departure, and during deep-space manoeuvres, but it is not checked continuously in between these events.

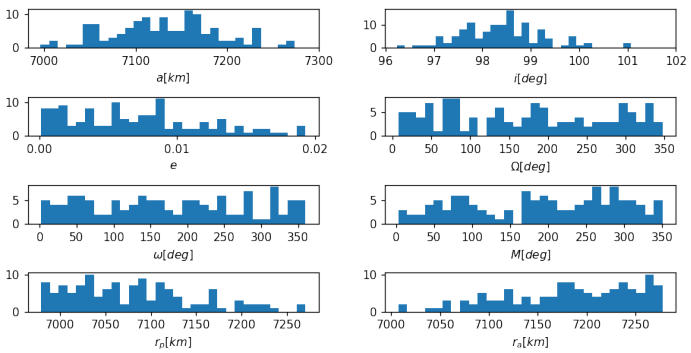

Figure 3.1: Orbital parameters of the M debris orbits [17]

3.1.1 JPL's solution

The winning JPL's solution consists of a 10-spacecraft campaign, operating sequentially over 8 years. The approach integrates several complementary techniques: branch-and-bound searches that leverage the natural drift of the right ascension of the ascending node to generate long rendezvous chains; beam-search strategies for

assembling full mission campaigns; Ant Colony Optimisation (ACO), and a genetic algorithm for exploring the combinatorial structure of the problem. In addition, transfer databases are constructed for all debris pairs over a finely discretised time grid, providing fast yet accurate estimates of the required transfer ΔV. Finally, a non-linear programming refinement is applied to guarantee that the resulting trajectories satisfy all mission constraints and are locally optimal with respect to the initial mass.
The JPL solution will be used as a comparison in subsequent analyses, in particular the total ΔV obtained of **25326** m/s [18].

Mission	Start MJD2000	End MJD2000	Launch Mass, kg	Number of objects	Debris ID	UTC
1	23557.18	23821.03	5665.38	14	23,55,79,113,25,20,27,117,121,50,95,102,38,97	20:17
2	23851.08	24024.53	4666.15	12	19,115,41,26,45,82,47,85,7,2,11,77	20:17
3	24057.47	24561.49	6589.58	21	72,107,61,10,28,3,64,66,31,90,73,87,57,35,69,65,8,43,71,4,29	21:42
4	24637.26	24916.44	5679.10	11	108,24,104,119,22,75,63,112,37,32,114	20:18
5	24946.47	25232.94	4906.59	14	84,59,98,1,40,51,36,67,62,99,54,122,76,15	20:18
6	25262.95	25455.15	5062.74	10	101,48,53,5,12,39,58,13,60,74	20:18
7	25485.20	25682.33	4082.33	10	49,9,70,93,105,46,88,118,18,91	20:18
8	25712.38	25915.53	3725.73	9	86,34,100,30,92,6,110,96,81	20:19
9	25946.06	26237.29	4897.35	12	33,68,116,106,14,52,120,80,16,94,83,89	20:19
10	26267.80	26416.00	3438.62	10	44,111,56,78,0,17,109,103,42,21	20:19

Figure 3.2: JPL's solution (campaign overview) [18]

Mission	ΔV, *m/s*
1	161.8,139.2,65.8,208.2,115.2,300.1,564.9,78.3,105.0,233.3,453.5,340.4,300.8
2	659.0,301.1,252.1,143.8,146.8,68.6,40.6,84.2,105.3,448.5,148.0
3	219.1,80.8,105.2,55.2,140.2,85.5,95.0,237.6,205.9,149.9,245.2,71.6,197.3,160.4,132.2,240.0,161.2,364.3,230.4,232.5
4	86.1,103.1,62.6,222.9,709.1,553.9,219.9,233.9,739.0,232.6
5	129.6,45.2,172.9,52.6,160.7,280.8,221.1,163.5,98.2,115.7,164.8,674.8,291.1
6	156.0,198.0,305.8,71.2,194.4,920.5,314.1,353.0,272.8
7	400.6,173.6,211.3,374.4,109.6,171.2,145.1,194.3,233.0
8	287.9,111.9,112.2,144.5,540.0,260.1,198.8,82.7
9	83.3,148.1,495.9,464.9,405.2,285.9,254.8,62.3,156.6,36.5,174.9
10	189.4,112.9,110.0,121.3,117.9,280.1,300.4,120.6,70.2

Figure 3.3: JPL's solution (ΔV) [18]

3.2 Changes to the problem

Compared to the formulation of the original GTOC9 problem, there are several differences in the study addressed in this thesis:

- the analyses only concerned the optimisation of ΔV, leaving out costs;
- the number of missions is set at 10, i.e. the number of missions in the winning solution;
- the time scale is discretised into 5-day intervals;

- the analytical model used for transfers allows bi-pulse or mono-pulse manoeuvres for each leg, unlike the original problem, which allows up to 5 pulses per leg.

3.3 Analytical model

Given the high combinatorial complexity of the problem, an analytical model is essential to obtain an accurate estimate of propulsive cost while keeping the computational burden manageable. The model employed is inspired by the approaches presented in [19] and [20].
Since the spacecraft operates in LEO, the J_2 perturbation is significantly stronger than any other disturbance and cannot be neglected. As mentioned in Section 2.2.2, the J_2 effect is not merely a source of difficulty: the differential nodal precession it induces can be exploited to reduce the cost of orbital plane changes. Plane–change manoeuvres are among the most propellant-demanding, becoming impractical for large inclination offsets (requiring approximately 1.3 km/s of ΔV per ten degrees [18]). Because the debris ascending nodes are distributed across the entire 360° range, as illustrated in Figure 3.1, leveraging J_2–driven nodal drift is crucial to keep manoeuvre costs within reasonable bounds.
This model only takes into account the secular effects of J_2, so the elements a, e, and i remain constant, whereas Ω, ω, and M evolve according to Equations 2.14, 2.15, and 2.16. The change in RAAN can be written as a function of small perturbations in the semi-major axis a and the inclination i as follows:

$$\frac{\delta\dot{\Omega}}{\dot{\Omega}} = \frac{\delta\dot{\Omega}/\delta a + \delta\dot{\Omega}/\delta i}{\dot{\Omega}} \tag{3.4}$$

replacing:

$$\frac{\delta\dot{\Omega}}{\delta a} = \frac{21}{4}\frac{\sqrt{\mu}}{a^{9/2}} r_E^2 J_2 \frac{\cos i}{(1-e^2)^2}\delta a \qquad \text{and} \qquad \frac{\delta\dot{\Omega}}{\delta i} = \frac{3}{2}\frac{\sqrt{\mu}}{a^{7/2}} r_E^2 J_2 \frac{\sin i}{(1-e^2)^2}\delta i$$

is then obtained:

$$\frac{\delta\dot{\Omega}}{\dot{\Omega}} = -\frac{7}{2}\frac{\delta a}{a} - \tan i \ \delta i \tag{3.5}$$

To evaluate the transfer cost, the analytical method requires the orbital elements of both the departure and arrival debris, as well as the epochs at the beginning and end of the transfer (denoted as t_s and t_a, respectively). The orbital elements necessary are specifically:

- the semi-major axes a_1 and a_2;
- the inclinations i_1 and i_2;
- the eccentricities e_1 and e_2;
- the RAAN values Ω_{ef1} and Ω_{ef2};
- the epochs at which these elements are evaluated, ep_1 and ep_2.

All these values are taken from the GTOC9 `.txt` file (see Appendix A).
We must therefore calculate the time required for the RAANs of the starting and ending debris to coincide:

$$\Delta t = -\frac{\Delta\Omega}{\Delta\dot{\Omega}} \tag{3.6}$$

The first step is to compute the RAAN drift rates ($\dot{\Omega}_1$ and $\dot{\Omega}_2$) for the two debris objects using Equation 2.14 and the RAAN values at the beginning of the transfer:

$$\begin{aligned} \Omega_{01} &= \dot{\Omega}_1 (t_s - ep_1) + \Omega_{ef1} \\ \Omega_{02} &= \dot{\Omega}_2 (t_s - ep_2) + \Omega_{ef2} \end{aligned} \tag{3.7}$$

After doing this, we can calculate the difference between the RAANs and the RAANs' rates of change of the two debris, to be substituted into Equation 3.6:

$$\begin{aligned} \Delta\Omega &= \Omega_{02} - \Omega_{01} \\ \Delta\dot{\Omega} &= \dot{\Omega}_2 - \dot{\Omega}_1 \end{aligned} \tag{3.8}$$

The value of Δt found in Equation 3.6, added to t_s, provides the arrival time $t = t_s + \Delta t$ for which the required RAAN change is zero.
The algorithm supports both single-pulse and double-pulse manoeuvres, evaluating the suitability of each and retaining only the best solution. The manoeuvres are:

- single-pulse at the beginning of the transfer leg, with:

$$\Delta v_a = \sqrt{x_0^2 + y^2 + z^2} \quad \Delta v_b = 0 \quad \text{with} \quad x_0 = \Delta\Omega \sin i_0 \; v_0 \tag{3.9}$$

- single-pulse at the end of the transfer leg, with:

$$\Delta v_a = 0 \quad \Delta v_b = \sqrt{x^2 + y^2 + z^2} \tag{3.10}$$

- double-pulse with ΔV optimally divided between the start and end of the transfer leg.

For the scenario with two pulses, if it falls within the case study without constraints on the transfer time between the two debris, the propulsion cost can be calculated directly as:

$$\Delta v_a = \Delta v_b = \frac{1}{2}\sqrt{y^2 + z^2} \tag{3.11}$$

It is generally unlikely to have no constraints on the duration of an orbital transfer, so if the transfer time may be different from Δt, as it often occurs, a manoeuvre is required to modify the RAAN as well. The first step is to determine the RAAN values of the starting and arrival debris (Ω_1 and Ω_2) at the arrival time t_a, and then we can extract $\Delta\Omega_{ar}$:

$$\begin{aligned} \Omega_1 &= \Omega_{01} + \dot{\Omega}_1(t_a - t_s) \\ \Omega_2 &= \Omega_{02} + \dot{\Omega}_2(t_a - t_s) \end{aligned} \quad \longrightarrow \quad \Delta\Omega_{ar} = \Omega_2 - \Omega_1 \tag{3.12}$$

The quantities x, y, and z are defined to represent the ΔV components required to modify the RAAN, the semi-major axis, and the inclination, respectively:

$$\begin{aligned} x &= \Delta\Omega_{ar}(\sin i_0)\, v_0 \\ y &= \frac{a_2 - a_1}{2a_0}\, v_0 \\ z &= (i_2 - i_1)\, v_0 \end{aligned} \quad \text{with} \quad \begin{aligned} i_0 &= (i_1 + i_2)/2 \\ a_0 &= (a_1 + a_2)/2 \\ v_0 &= \sqrt{\mu/a_0} \end{aligned} \tag{3.13}$$

The first impulse performs a partial correction of the quantities x, y, and z (with s_x, s_y, and s_z denoting the corresponding fractions) while the second impulse completes the remaining adjustments. It is important to note that fuel-efficient solutions generally favour **combined manoeuvres**. The first velocity impulse Δv_a is expressed as follows:

$$\Delta v_a = \sqrt{(s_x x)^2 + (s_y y)^2 + (s_z z)^2} \tag{3.14}$$

Typically, the goal of a manoeuvre is to achieve the exact desired values of a and i. However, the model allows these parameters to exceed the target values temporarily. Although this may seem counterintuitive, it is actually a strategic choice. Since the J_2 term depends directly on a and i, their variation can alter the precession rate of the ascending node, promoting a more favourable alignment between the orbital planes and thereby reducing the overall cost of the manoeuvre. Changing the semi-major axis and inclination produces a difference (Δx) in the RAAN during the transfer, which we can derive starting from:

$$\begin{aligned} \delta\dot{\Omega} &= -\frac{7}{2}\frac{\delta a}{a_0}\dot{\Omega}_0 - \tan i_0\ \delta i\ \dot{\Omega}_0 \\ \delta\Omega &= \delta\dot{\Omega} \cdot t = -\frac{7}{2}\frac{\delta a}{a_0}\dot{\Omega}_0 t - \tan i_0\ \delta i\ \dot{\Omega}_0\ t \end{aligned} \tag{3.15}$$

where $\dot{\Omega}_0 = (\dot{\Omega}_1 + \dot{\Omega}_2)/2$ is the average RAAN change rate of the starting and arrival debris. Substituting in the x formulation of Equation 3.13, we obtain:

$$\Delta x = -\frac{7}{2}\dot{\Omega}_0 \frac{\delta a}{a_0} v_0 \ \sin i_0 \ t - \dot{\Omega}_0 \tan i_0 \ \delta i \ v_0 \ \sin i_0 \ t \tag{3.16}$$

Finally, using the y and z formulations of Equation 3.13, we get:

$$\Delta x = 7\dot{\Omega}_0 \ \sin i_0 \ t \ s_y \ y + \dot{\Omega}_0 \tan i_0 \ \sin i_0 \ t \ s_z \ z = m \ s_y \ y + n \ s_z \ z \tag{3.17}$$

Calculating the second impulse Δv_b of the manoeuvre as:

$$\Delta v_b = \sqrt{(x - s_x x - \Delta x)^2 + (y + s_y y)^2 + (z + s_z z)^2} \tag{3.18}$$

the total ΔV can be calculated:

$$\begin{gathered} \Delta V = \Delta v_a + \Delta v_b = \\ = \sqrt{(s_x x)^2 + (s_y y)^2 + (s_z z)^2} + \sqrt{(x - s_x x - \Delta x)^2 + (y + s_y y)^2 + (z + s_z z)^2} \end{gathered} \tag{3.19}$$

At this stage, the next step is to determine the optimal values of s_x, s_y, and s_z. Because finding the minimum of ΔV in closed form is challenging, an analytical approximation can be employed by squaring the two velocities to eliminate the square root and by neglecting the cross-product terms $2\Delta v_a \Delta v_b$ [19]:

$$\begin{gathered} \Delta v_a^2 + \Delta v_b^2 = \\ (s_x x)^2 + (s_y y)^2 + (s_z z)^2 + (x - s_x x - \Delta x)^2 + (y + s_y y)^2 + (z + s_z z)^2 \end{gathered} \tag{3.20}$$

Next, we compute the partial derivatives with respect to the relevant parameters and set them to zero to determine their optimal values:

$$\begin{aligned} \frac{\partial (\Delta v_a^2 + \Delta v_b^2)}{\partial s_x} &= 4 s_x x^2 - 2x^2 + 2mxs_y y + 2nxs_z z = 0 \\ \frac{\partial (\Delta v_a^2 + \Delta v_b^2)}{\partial s_y} &= 4 s_y y^2 + 2m^2 s_y y^2 + 2mxs_y y + 2mnys_z z + 2y^2 - 2mxy = 0 \\ \frac{\partial (\Delta v_a^2 + \Delta v_b^2)}{\partial s_z} &= 4 s_z z^2 + 2n^2 s_z z^2 + 2nxs_z z + 2mns_y y + 2z^2 - 2nxz = 0 \end{aligned} \tag{3.21}$$

Finally, solving the system of equations gives:

$$
\begin{aligned}
s_x &= \frac{2x + my + nz}{(4 + m^2 + n^2)\, x} \\
s_y &= \frac{2mx - (4 + n^2)\, y + mnz}{(8 + 2m^2 + 2n^2)\, y} \\
s_z &= \frac{2nx + mny - (4 + m^2)\, z}{(8 + 2m^2 + 2n^2)\, z}
\end{aligned}
\tag{3.22}
$$

These values, substituted into Equation 3.19, allow us to obtain the optimal division of the two pulses.

Chapter 4

Ant Colony Optimisation

The problem analysed and presented in Section 3 is a combinatorial optimisation problem associated with the famous **Travelling Salesman Problem** (TSP).
Combinatorial optimisation problems require determining values for discrete variables in such a way that the solution is optimal with respect to a specified objective function. Such problems may be formulated either as maximisation or minimisation tasks, each associated with a collection of possible instances. These problems are particularly challenging because, although they are typically simple to describe, they are often complicated to solve. Many practical problems of this type are $\mathcal{NP}$-hard, meaning that it is widely believed that no algorithm can solve them to optimality within computation times bounded by a polynomial function. As a result, when dealing with large instances, one must generally rely on approximate techniques that produce near-optimal solutions within a reasonable amount of time. Algorithms of this nature are commonly referred to as heuristics.
A **metaheuristic** consists of a set of algorithmic principles that can be used to design heuristic strategies to obtain high-quality solutions to complex and practically important combinatorial optimisation problems within acceptable computational times. The **Ant Colony Optimisation** (ACO) algorithm, implemented in this thesis, is one of them [21].

4.1 Travelling Salesman Problem

The Travelling Salesman Problem (TSP) concerns a salesman who, starting from his home city, seeks to determine the shortest possible route that allows him to visit a given set of customer cities exactly once and then return to the point of origin. The TSP can be modelled as a complete weighted graph $G = (N, A)$, where N is the set of nodes (cities), with $n = |N|$, and A is the set of arcs fully connecting all node pairs. Each arc $(i, j) \in A$ is associated with a weight d_{ij}, representing

the distance between cities i and j. The objective of the TSP is to identify a Hamiltonian circuit of **minimum total length**, where a Hamiltonian circuit is defined as a closed tour that visits every node in G exactly once.
The TSP is a paradigmatic $\mathcal{NP}$-hard combinatorial optimisation problem. A natural strategy for solving combinatorial optimisation problems is to enumerate all feasible solutions and select the best one. However, this brute-force approach quickly becomes impractical, as the number of possible solutions increases exponentially with the problem's size.
A key theoretical framework for assessing the difficulty of combinatorial problems is $\mathcal{NP}$-completeness, which divides such problems into two broad categories:

- $\mathcal{P}$: problems for which there exists an algorithm that returns the correct *yes* or *no* answer in polynomial time;
- $\mathcal{NP}$: problems for which a given *yes* answer can be verified in polynomial time, regardless of how the instance was generated.

Two main families of algorithms can be employed to solve combinatorial optimisation problems: **exact** and **approximate** methods. Exact algorithms are guaranteed to determine the optimal solution and prove its optimality for any finite instance. When optimal solutions cannot be computed efficiently, it can be useful to trade optimality for computational feasibility. This means accepting algorithms that produce high-quality, even if not necessarily optimal, solutions within polynomial time. These approximate algorithms, commonly referred to as heuristics or heuristic methods, aim to deliver near-optimal results at a relatively low computational cost without providing any formal guarantee of optimality [21].

4.2 Real ants behaviour

The field of ant algorithms investigates models derived from the observation of real ants' behaviour and uses them as inspiration for designing new algorithms to solve optimisation problems. The central idea is that the self-organising principles enabling the highly coordinated behaviour of ant colonies can be exploited to coordinate populations of artificial agents that collaborate to solve computational tasks. In particular, during foraging activities, ants coordinate their behaviour through **stigmergy**, a form of indirect communication mediated by environmental modifications. For example, a foraging ant deposits a chemical on the ground, increasing the probability that other ants will follow the same path. This chemical communication is mainly based on **pheromones**, substances produced by ants that enable them to interact with one another and with the environment. A key element in the social organisation of several ant species is the **trail pheromone**, a specific

type of pheromone used to mark paths on the ground, such as those connecting food sources to the nest. This constitutes the principal source of inspiration for ant algorithms [21].

4.2.1 Double Bridge experiments

The behaviour of ants was studied using three variants of the **Double Bridge experiment**: in the first variant, the ants had two paths of equal length available to them; in the second, two paths of different lengths; and in the last variant, they initially had only the longer path and only subsequently the shorter one.

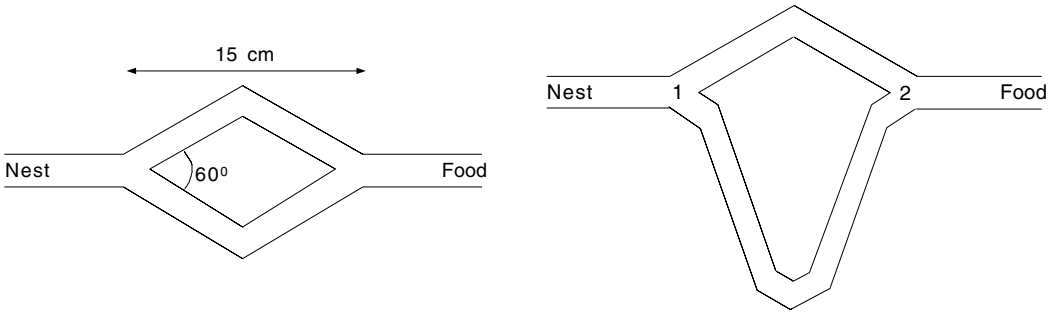

(a) Equal lenght **(b)** Different lenght

Figure 4.1: Experiment setup [21]

Ants release pheromones onto the ground as they move between the nest and food sources, thereby creating chemical trails. These trails can be detected by other ants, which are more likely (according to a probabilistic decision process) to follow paths characterised by higher pheromone concentrations.
At the beginning of the first experiment, there is obviously no trace of pheromone, so the ants begin to walk across the two bridges randomly. Subsequently, due to random fluctuations, a greater number of ants travel along the same path, increasing the pheromone concentration there and leading other ants to follow. This behaviour is known as **autocatalytic** or **positive feedback**. Although there is no advantage in choosing one path over another, the ants converge on a single choice. However, some individuals continue to travel along the other bridge, displaying **exploratory** behaviour.
At the beginning of the second experiment, the ants also began to travel the two paths randomly, but in this scenario, the ants eventually converged on the use of the shorter branch. Since one branch is shorter than the other, the ants that initially select the shorter path are also the first to reach the food source and begin the

return journey to the nest. When they face the choice between the short and long branch on their way back, the higher pheromone concentration on the shorter path biases their decisions toward it. As a consequence, pheromone accumulates more rapidly on the short branch, which, through the previously described autocatalytic mechanism, becomes the route ultimately adopted by the entire colony. Even in this case, despite being disadvantageous, some ants continued to follow the longer route.
In the latter case, the shortest route is only added later, so the ants are already travelling the longer route. In this situation, the shorter branch was chosen only occasionally, and the colony remained confined to the longer branch. This outcome can be attributed to the high pheromone concentration already present on the long branch and to the slow rate of pheromone evaporation. Because of the strong pheromone signal, most ants continued to select the long path, and this autocatalytic mechanism further strengthened its attractiveness, even when a shorter alternative became available. The **evaporation** process, which in principle could promote the exploration of new routes, was too slow to counteract this effect, as the pheromone persisted for a duration comparable to that of the entire trial [21].

4.3 Metaheuristic

A metaheuristic is a collection of algorithmic principles that can be employed to design heuristic methods suitable for a broad range of different problems. In essence, a metaheuristic is a general-purpose framework that guides a problem-specific heuristic toward promising areas of the search space where high-quality solutions are likely to be found. ACO is a metaheuristic in which a population of artificial ants collaborates to discover reasonable solutions to complex discrete optimisation problems. Cooperation constitutes a fundamental design aspect of ACO algorithms.
In ACO, an artificial ant is a stochastic constructive procedure that builds a solution incrementally by adding appropriately defined components to the partial solution under construction. The ACO algorithm can be understood as the interaction of three main procedures:

- the **Construction of the solution** procedure coordinates a colony of ants that explore neighbouring states of the problem by moving across adjacent nodes of the problem's construction graph;
- the **Update of the pheromones** procedure handles the modification of pheromone trails. These values may increase through pheromone deposition on the solution components or connections used by the ants, or decrease as a consequence of pheromone evaporation;

- the **Daemon actions** procedure enables the execution of centralised operations that individual ants cannot perform autonomously. Examples include activating a local optimisation routine or gathering global information that may suggest whether it is advantageous to add extra pheromone to influence the search from a non-local perspective. This step is optional.

4.4 Ant System and Travelling Salesman Problem

4.4.1 Tour construction

At the start of the process, the ants are placed on cities selected at random. During each step of the tour construction, ant k uses a probabilistic decision mechanism known as the **random proportional rule** to determine the next city to visit. Specifically, the probability that ant k, currently located in city i, will move to city j is given by:

$$p_{ij}^k = \frac{(\tau_{ij})^\beta (\eta_{ij})^\alpha}{\Sigma_{l \in N_i^k} (\tau_{il})^\beta (\eta_{il})^\alpha}, \quad \text{if } j \in N_i^k \tag{4.1}$$

where $\eta_{ij} = 1/d_{ij}$ represents the heuristic value known in advance and τ_{ij} the pheromone trail that refers to the desirability of visiting city j directly after city i. The parameters β and α control the relative influence of the pheromone trail and the heuristic information, respectively; and N_i^k denotes the feasible neighbourhood of ant k when located at city i, that is, the set of cities that the ant has not yet visited.
According to this probabilistic decision rule, the likelihood of selecting a specific arc (i, j) increases with the amount of pheromone τ_{ij} deposited on it and with the magnitude of the heuristic value η_{ij}. The parameters α and β play distinct roles: when $\beta = 0$, ants tend to favour the nearest cities, effectively reducing the behaviour to a classical stochastic greedy algorithm. Conversely, if $\alpha = 0$, decisions rely solely on pheromone reinforcement, with no heuristic contribution. This typically produces suboptimal performance and, for values $\beta > 1$, often results in a rapid onset of stagnation [21]. Further information on this can be found in the Section 5.1. Please note that, compared to the classical definition, the parameters α and β are inverted.

4.4.2 Update of pheromone trace

After all ants have completed their tours, the pheromone levels on the paths are updated. The update process begins by reducing the pheromone concentration

on every arc by a fixed evaporation factor, after which additional pheromone is deposited on the arcs that the ants traversed during their tours. The evaporation mechanism is applied by:

$$\tau_{ij} \leftarrow (1-\rho)\tau_{ij} \quad \forall (i,j) \in A \tag{4.2}$$

In the above equation, ρ ($0 < \rho \leq 1$) represents the pheromone evaporation rate. This parameter is fundamental because it prevents the pheromone levels from growing without limit and allows the algorithm to forget previously made suboptimal choices. Indeed, if any ant does not select an arc, its pheromone concentration decreases over time. Once evaporation has taken place, each ant deposits new pheromone on the arcs included in its tour:

$$\tau_{ij} \leftarrow \tau_{ij} + \sum_{k=1}^{n} \Delta\tau_{ij}^{k} \quad \forall (i,j) \in A \tag{4.3}$$

τ_{ij} denotes the quantity of pheromone that the ant k releases on the arcs it has traversed. This quantity is defined as follows:

$$\Delta\tau_{ij}^{k} = \begin{cases} \frac{1}{C^k} & \text{if arc}(i,j) \text{ belongs to } T^k \\ 0 & \text{otherwise} \end{cases} \tag{4.4}$$

In this expression, C_k is the length of the tour T_k constructed by the k-th ant, and it is obtained by summing the lengths of all arcs included in T_k. The underlying principle is that the higher the quality of an ant's tour, the greater the amount of pheromone deposited on the corresponding arcs. Consequently, arcs selected by many ants and belonging to relatively short tours accumulate higher pheromone levels, making them more likely to be chosen in subsequent iterations of the algorithm [21].

Chapter 5

Analysis

This chapter presents and discusses the key results obtained from applying the ACO algorithm to the GTOC9 case study. The objective is to evaluate its performance relative to the JPL benchmark and examine how the algorithm behaves under varying parameter settings. It's important to highlight that the mission scenario developed by the JPL for the removal of 123 debris objects specified in the competition assumes a total ΔV of **25326 m/s**.

5.1 Features of the algorithm

5.1.1 Matrices

A key feature of the algorithm is the 4-D cost matrix, which measures the propulsion costs required to transfer between different pieces of debris. Creating this matrix requires knowledge of each object's orbital parameters and involves calculating the ΔV required for each orbital manoeuvre. Thus, the resulting matrix contains the costs associated with the transfer between each pair of debris for all possible departure times and all considered durations. Each element is expressed in the following manner:

$$d(i,\ j,\ t_p,\ \Delta t)$$

where i is the starting debris, j is the arrival debris, t_p is the starting time, sampled every 5 days over the entire duration of the campaign, and Δt is the transfer duration, expressed as a multiple of 5 days in the range 5-30.
The heuristic matrix is then derived, defining the desirability of transfers and serving as a fundamental component of the ants' solution-construction phase. Each element of the heuristic matrix is expressed as:

$$h(i,\ j,\ t_p,\ \Delta t) = \frac{1}{d(i,\ j,\ t_p,\ \Delta t)}$$

Another matrix of fundamental importance is the pheromone matrix, an $n \times n$ matrix (where n is the number of debris considered) containing the pheromone left by the ants after their tour.

5.1.2 Parameters

As mentioned above, the algorithm is highly influenced by the chosen parameters, resulting in very different outcomes. Therefore, careful selection is essential. The parameters are:

- number of iterations **miter**;
- number of ants **n**;
- weight attributed to heuristic information $\boldsymbol{\alpha}$;
- weight attributed to the pheromone $\boldsymbol{\beta}$;
- pheromone's evaporation rate **e**;
- pheromone's deposition rate $\boldsymbol{\delta t}$;
- common cost elimination **el**.

The pheromone deposition rate is calculated as:

$$\delta t = \frac{dt}{f_i} \tag{5.1}$$

where dt is a parameter and f_i is a quantity relative to the i-th ant calculated as:

$$f_i = \frac{cost_i}{min(cost)} - el \quad \text{or} \quad f_{i,var} = cost_i - el \cdot min(cost) \tag{5.2}$$

where $cost_i$ is the cost in term of ΔV of the i-th tour, $min(cost)$ is the minimum cost among all the n tours.
An optimal choice of parameters not only influences the quality of the solution but also the computational cost required to obtain it. The parameters were initially set to specific values based on the studies of [20] and [22]. In particular, the optimal values of β are around unity. Higher values tend to cause the algorithm's search to stagnate quickly, without finding acceptable solutions. As for the parameter α, with values below unity, especially near zero, the algorithm tends to find poor solutions,

as insufficient weight is given to heuristics. The best solutions are obtained for values greater than unity, but not excessively so, as excessively high values can lead to stagnation. The evaporation rate must be between 0 and 1, with the right balance between memory of old paths and new explorations in the vicinity of $e = 0.5$.
As a reference for computational cost, all analyses were performed on a PC with an AMD Ryzen 5 7500F 3.7 GHz processor and 32 GB of DDR5 6000 MHz RAM.

5.2 First iterations

The purpose of the initial analyses is to examine the algorithm's behaviour as the "secondary" parameters vary. Each problem has unique characteristics, so even though it can be linked to a TSP solved using ACO, the study of the parameters carried out in [22] may not be fully applicable. In fact, based on the study carried out in [20], it was decided to set $\alpha = 4$ and $\beta = 1$. To be on the safe side, a study was also conducted with other parameter combinations, but the results (not reported) confirmed the initial choice of parameters.

5.2.1 Number of ants

A fundamental analysis concerns the number of ants, another parameter that directly influences the problem. Various trials were conducted with different parameter sets, considering $n = m$ and $n = 4m$ ants, where $m = 123$ is the number of debris in the problem under analysis. Each trial was carried out with the number of repetitions of the ACO algorithm $miter = 100$. In the following tables, the costs are a function of ΔV, in particular:

- Min represents the minimum cost over 100 iterations;
- $Aver$ represents the average of the minimum costs of each iteration;
- Avg (if present) represents the average of the averages obtained with a set of parameters.

The outcomes of the initial analysis for the two ant groups are displayed in Table 5.1 and Table 5.2. For each ant set, the most optimal and least favourable results were identified based on the average of the minimum ΔV values across each iteration.
Regarding case $n = m$, trials **A0** and **A4** (Figure 5.1):

Caso	$\boldsymbol{\alpha}$	$\boldsymbol{\beta}$	**el**	**dt**	**e**	**Min**	**Aver**
A0	4	1	0.99	0.01	0.05	5.17E + 04	5.78E + 04
A1	4	1	0.99	0.007	0.05	5.26E + 04	5.80E + 04
A2	4	1	0.995	0.007	0.15	5.17E + 04	5.88E + 04
A3	4	1	0.999	0.007	0.15	5.33E + 04	5.84E + 04
A4	4	1	0.999	0.007	0.05	5.36E + 04	6.15E + 04
A5	4	1	0.999	0.007	0.1	5.28E + 04	6.07E + 04
A6	4	1	0.995	0.007	0.1	5.46E + 04	5.99E + 04

Table 5.1: Initial analysis: $n = m$

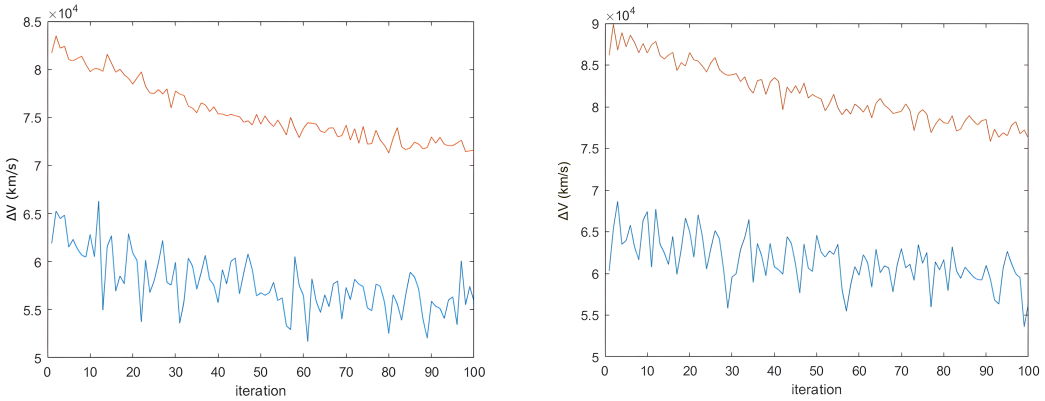

(a) Trial A0 **(b)** Trial A4

Figure 5.1: Initial analysis: n = m, best and worst trial

Regarding case $n = 4m$, trials **B4** and **B2** (Figure 5.2):

Trial	$\boldsymbol{\alpha}$	$\boldsymbol{\beta}$	**el**	**dt**	**e**	**Min**	**Aver**
B0	4	1	0.99	0.01	0.05	5.02E + 04	5.58E + 04
B1	4	1	0.99	0.007	0.05	4.98E + 04	5.60E + 04
B2	4	1	0.99	0.001	0.05	5.09E + 04	5.83E + 04
B3	4	1	0.99	0.09	0.05	5.00E + 04	5.53E + 04
B4	4	1	0.99	0.05	0.05	4.76E + 04	5.50E + 04
B5	4	1	0.99	0.03	0.05	5.21E + 04	5.72E + 04
B6	4	1	0.99	0.07	0.05	4.92E + 04	5.63E + 04

Table 5.2: Initial analysis: $n = 4m$

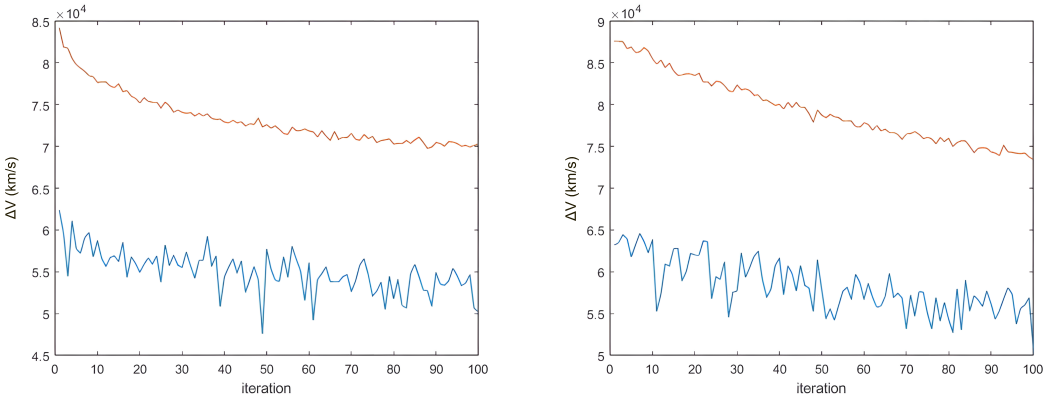

(a) Trial B4 **(b)** Trial B2

Figure 5.2: Initial analysis: n = 4m, best and worst trial

In the Figure 5.1 and 5.2, and in all subsequent graphs of this type, the blue line represents the minimum ΔV trend for each iteration, while the orange line represents the average trend.
In the first case, the differences between the best and worst trial concern the parameters *el* and *dt*, which mutually influence δt (Equation 5.1), with *el* increasing slightly and *dt* decreasing by an order of magnitude. The increase in *el* causes a decrease in f_i (Equation 5.2), which leads to an increase in δt. Elevating the amount of pheromone released could cause the algorithm to converge too quickly towards suboptimal solutions, so we attempted to mitigate this by decreasing *dt*. A moderate pheromone deposit leads to a more exploratory algorithm, increasing the likelihood of finding an optimal solution. However, if after many iterations all solutions carry similar pheromone levels, no solution would stand out. In the second case, the only change between the best and worst trials was a reduction in the *dt* parameter, which led to worse outcomes. Excessively reducing the pheromone deposit worsens the solutions obtained.
It should be noted that the observed behaviour is ideal, as the average cost is initially higher due to a still-low pheromone trail, leading to greater exploration by the ants. As the iterations increase, the average cost decreases as the ants begin to prefer the most efficient paths. The main difference is that in the two worst cases, the trend of the average ΔV is more linear.
Since the two cases are quite similar, differing only in *dt* and the number of ants n, a more in-depth study of the parameters was conducted based on these two trials. All analyses show very similar behaviour, but it is clear that analyses performed with $n = 4m$ provide better results for any set of parameters. When comparing the two most successful trials (Figure 5.3), obtained using an identical set of parameters, it becomes immediately evident that the case with $n = 4m$ exhibits a more stable

average trend and, most notably, a significantly improved minimum trend,

Trial	$\boldsymbol{\alpha}$	$\boldsymbol{\beta}$	**el**	**dt**	**e**	**Min**	**Aver**	**Avg**
A0.0	4	1	0.99	0.01	0.05	5.17E + 04	5.78E + 04	
A0.1	4	1	0.99	0.01	0.05	5.11E + 04	5.81E + 04	5.83E + 04
A0.2	4	1	0.99	0.01	0.05	5.20E + 04	5.90E + 04	
A0.3	4	1	0.99	0.01	0.1	4.95E + 04	5.86E + 04	
A0.4	4	1	0.99	0.01	0.1	5.36E + 04	6.00E + 04	5.93E + 04
A0.5	4	1	0.99	0.01	0.1	5.21E + 04	5.92E + 04	
A0.6	4	1	0.999	0.05	0.1	5.21E + 04	5.88E + 04	
A0.7	4	1	0.999	0.05	0.1	4.97E + 04	5.72E + 04	5.76E + 04
A0.8	4	1	0.999	0.05	0.1	5.04E + 04	5.70E + 04	
A0.9	4	1	0.999	0.007	0.1	5.39E + 04	5.94E + 04	
A0.10	4	1	0.999	0.007	0.1	5.10E + 04	5.80E + 04	5.90E + 04
A0.11	4	1	0.999	0.007	0.1	5.25E + 04	5.96E + 04	

Table 5.3: Second analysis: $n = m$

Trial	$\boldsymbol{\alpha}$	$\boldsymbol{\beta}$	**el**	**dt**	**e**	**Min**	**Aver**	**Avg**
B4.0	4	1	0.99	0.05	0.05	4.76E + 04	5.50E + 04	
B4.1	4	1	0.99	0.05	0.05	4.96E + 04	5.58E + 04	5.55E + 04
B4.2	4	1	0.99	0.05	0.05	4.88E + 04	5.57E + 04	
B4.3	4	1	0.99	0.05	0.1	4.91E + 04	5.59E + 04	
B4.4	4	1	0.99	0.05	0.1	4.96E + 04	5.47E + 04	5.52E + 04
B4.5	4	1	0.99	0.05	0.1	4.96E + 04	5.51E + 04	
B4.6	4	1	0.999	0.05	0.05	4.43E + 04	5.54E + 04	
B4.7	4	1	0.999	0.05	0.05	4.60E + 04	5.42E + 04	5.55E + 04
B4.8	4	1	0.999	0.05	0.05	5.06E + 04	5.67E + 04	
B4.9	4	1	0.999	0.05	0.1	4.83E + 04	5.15E + 04	
B4.10	4	1	0.999	0.05	0.1	4.81E + 04	5.36E + 04	5.36E + 04
B4.11	4	1	0.999	0.05	0.1	4.80E + 04	5.55E + 04	
B4.12	4	1	0.999	0.007	0.1	4.90E + 04	5.52E + 04	
B4.13	4	1	0.999	0.007	0.1	4.85E + 04	5.60E + 04	5.59E + 04
B4.14	4	1	0.999	0.007	0.1	5.13E + 04	5.64E + 04	

Table 5.4: Second analysis: $n = 4m$

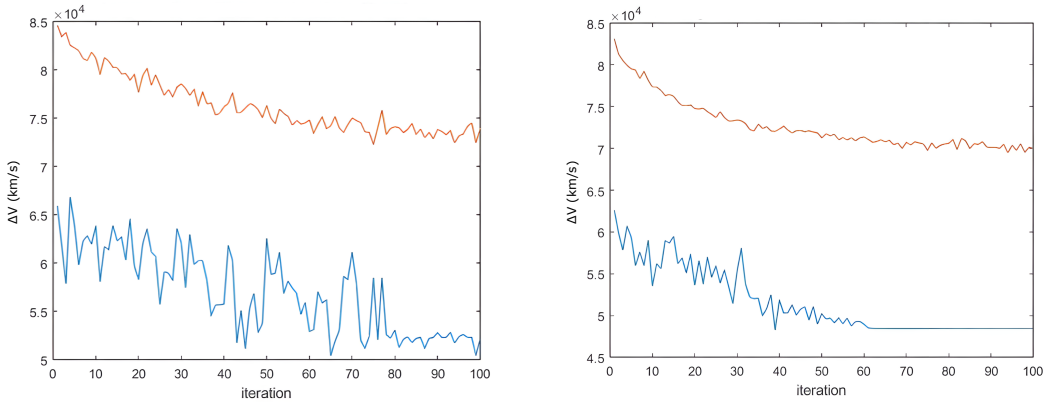

(a) Trial A0.8 **(b)** Trial B4.9

Figure 5.3: Second analysis: best trials

characterised by fewer oscillations and a rapid decline. Although the trend flattens after the 60th iteration, subsequent iterations will utilise this trial as a reference benchmark. Having more ants increases the computational cost of the analyses, from about $1 \div 2$ minutes for $n = m$ to about $3 \div 7$ minutes for $n = 4m$, but the better results justify the increase.

5.2.2 Pheromone matrix study

To gain a clearer understanding of how the pheromone deposition evolves during the optimisation process, as well as to better assess the influence of the parameter e, a dedicated analysis was carried out on the $t1k$ pheromone matrices. These matrices, updated at every iteration, provide a detailed representation of how the ants collectively shape the search space through their choices. For each iteration, the maximum pheromone value within every row was identified, and attention was directed toward determining how many cells reached at least 10% of this maximum value. This threshold, although seemingly small, is actually meaningful: the large number of ants involved in the process implies that even transitions with comparatively low pheromone intensity may still be selected. Consequently, tracking how many cells remain above this modest percentage offers insight into how widely the algorithm continues to explore the surrounding solution space.
A closer look at the ΔV values reported in Tables 5.5 and 5.6 reveals no clear trend: there is a slight decrease in the minimum values and a slight increase in the average values for the case with a lower evaporation coefficient. Examining the number of cells in the threshold in Tables B.1 and B.2, it is evident that the case with reduced pheromone evaporation has more cells. Trials where fewer cells exceed this threshold in the final iterations tend to produce better optimisation results. This

behaviour suggests a more decisive and well-guided search process: the algorithm progressively concentrates pheromone on the most promising transitions, allowing them to stand out distinctly from less favourable ones. Lower evaporation preserves ant paths more effectively, leading to excessive amplification of suboptimal paths. This could explain the increase in average values.

Trial	$\boldsymbol{\alpha}$	$\boldsymbol{\beta}$	**el**	**dt**	**e**	**Min**	**Aver**
T1	4	1	0.999	0.05	0.1	5.23E + 04	5.80E + 04
T2	4	1	0.999	0.05	0.1	4.74E + 04	5.45E + 04
T3	4	1	0.999	0.05	0.1	4.84E + 04	5.56E + 04
T4	4	1	0.999	0.05	0.1	4.89E + 04	5.58E + 04
T5	4	1	0.999	0.05	0.1	4.98E + 04	5.44E + 04
T6	4	1	0.999	0.05	0.1	5.00E + 04	5.56E + 04
T7	4	1	0.999	0.05	0.1	4.87E + 04	5.47E + 04
T8	4	1	0.999	0.05	0.1	4.94E + 04	5.55E + 04
T9	4	1	0.999	0.05	0.1	5.07E + 04	5.58E + 04
T10	4	1	0.999	0.05	0.1	5.25E + 04	5.73E + 04
Average						4.98E + 04	5.57E + 04

Table 5.5: Case B4.9: t1k first analysis

Trial	$\boldsymbol{\alpha}$	$\boldsymbol{\beta}$	**el**	**dt**	**e**	**Min**	**Aver**
T1b	4	1	0.999	0.05	0.01	5.00E + 04	5.68E + 04
T2b	4	1	0.999	0.05	0.01	5.09E + 04	5.59E + 04
T3b	4	1	0.999	0.05	0.01	5.00E + 04	5.63E + 04
T4b	4	1	0.999	0.05	0.01	5.16E + 04	5.74E + 04
T5b	4	1	0.999	0.05	0.01	4.47E + 04	5.46E + 04
Average						4.94E + 04	5.62E + 04

Table 5.6: Case B4.9: analysis with $e = 0.01$

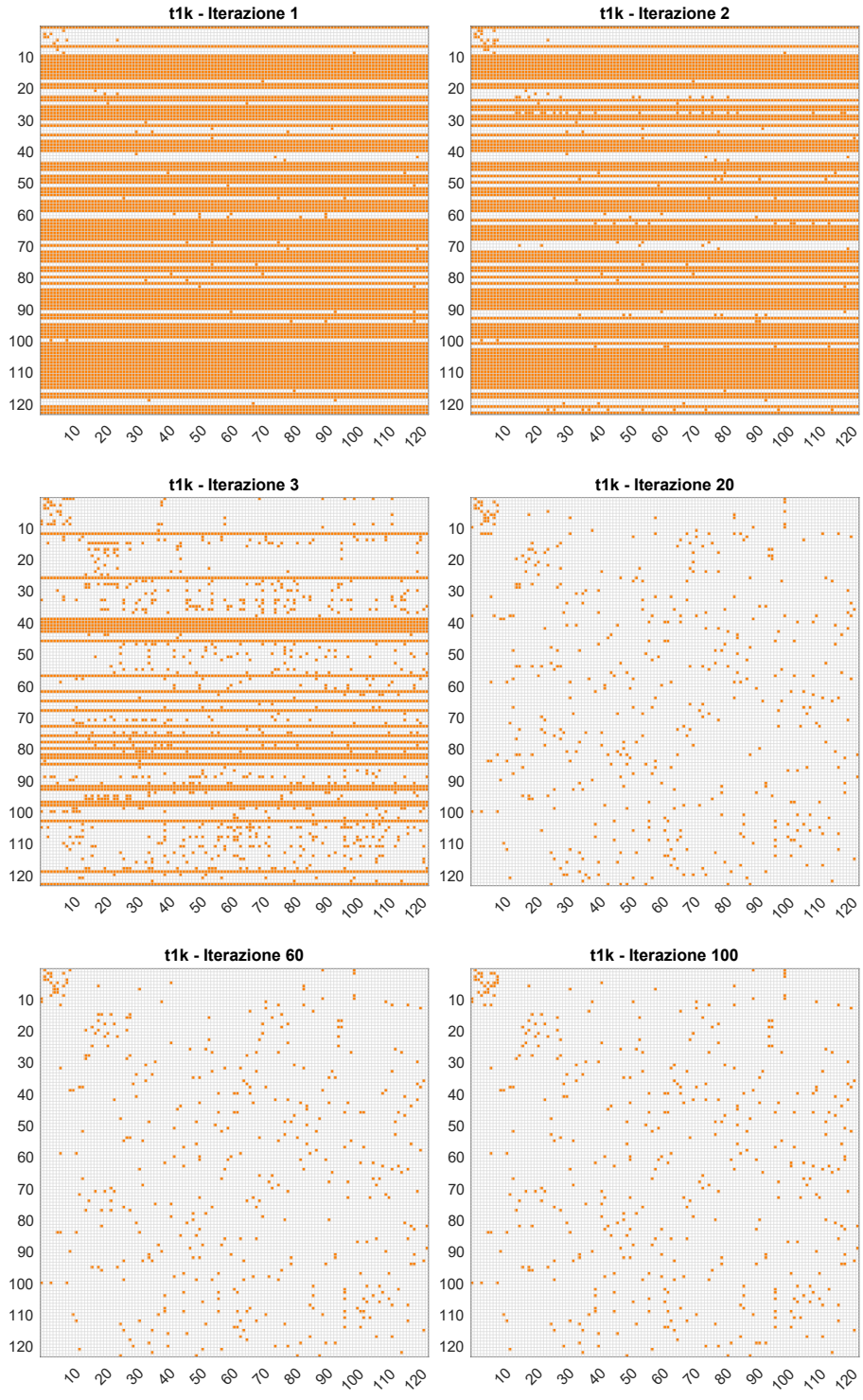

Figure 5.4: Trial T3: pheromone matrix

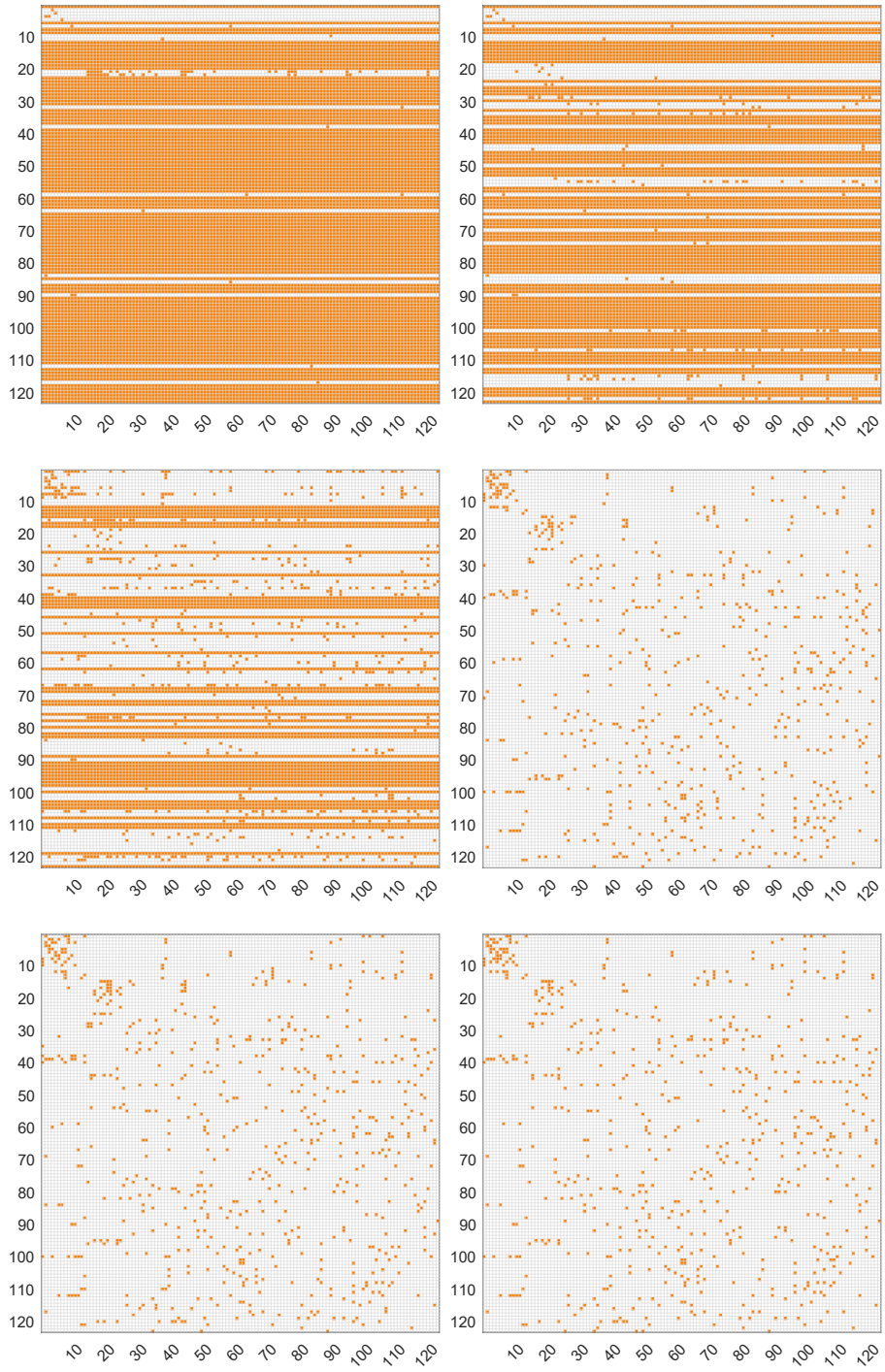

Figure 5.5: Trial T2b: pheromone matrix

5.3 Change in the calculation of f

To evaluate the influence of the cost update function f (see Equation 5.2) on the overall behaviour of the algorithm, additional tests were carried out employing both formulations available in the *calculate_cost* function of the code. This routine computes the total cost of the tour constructed by each ant during a given iteration, accounting for the cumulative effect of all transitions along the path. The function outputs the cost vector f, whose elements serve as the key reference quantities for the subsequent stage of the optimisation process. As such, understanding how the different formulations of f shape these values is essential for interpreting their impact on the algorithm's convergence properties and on the quality of the solutions obtained. Preliminary analyses using the alternative formulation of f (not shown here) yielded results that were noticeably inferior to those obtained with the standard configuration. A more careful examination revealed that a substantial increase in the parameter dt, and consequently in the amount of pheromone deposited at each iteration, resulted in a marked performance improvement. This behaviour suggests that the modified cost function may require a stronger reinforcement mechanism to compensate for its reduced effectiveness, enabling the algorithm to distinguish promising solutions better and guide the search toward higher-quality trajectories.

Trial	$\boldsymbol{\alpha}$	$\boldsymbol{\beta}$	**el**	**dt**	**e**	**Min**	**Aver**
T1f	4	1	0.999	1.5	0.1	4.92E + 04	5.58E + 04
T2f	4	1	0.999	1.5	0.1	5.15E + 04	5.81E + 04
T3f	4	1	0.999	1.5	0.1	5.09E + 04	5.76E + 04
T4f	4	1	0.999	1.5	0.1	4.92E + 04	5.67E + 04
T5f	4	1	0.999	1.5	0.1	5.05E + 04	5.73E + 04
Average						5.02E + 04	5.71E + 04
T6f	4	1	0.999	1.5	0.01	5.42E + 04	5.95E + 04
T7f	4	1	0.999	1.5	0.01	5.28E + 04	6.00E + 04
T8f	4	1	0.999	1.5	0.01	5.08E + 04	5.83E + 04
T9f	4	1	0.999	1.5	0.01	5.19E + 04	5.82E + 04
T10f	4	1	0.999	1.5	0.01	5.29E + 04	5.92E + 04
Average						5.25E + 04	5.91E + 04

Table 5.7: Case f_{var}: analysis with $dt = 1.5$

In this case, it is even more evident what was observed in the previous set of analyses, namely that reducing the value of the parameter e consistently led to a

deterioration in the quality of the results. The deterioration can be easily explained by looking at Table B.3: for lower e, there is no predominant choice, and all cells remain within the analysis range (at least 10% of the maximum pheromone value). This confirms the earlier conclusion that lower evaporation rates weaken the algorithm's ability to discriminate effectively between promising and non-promising paths, thereby hindering convergence toward high-quality solutions. Given the repeatability of this behaviour across different experimental configurations, the reduced e setting is deemed unsuitable for this study and will therefore be excluded from all subsequent analyses.
By further increasing the amount of pheromone deposited at each iteration, the algorithm achieves progressively better outcomes, reaching minimum values that are essentially comparable to those obtained in the standard configuration. However, the average values remain consistently higher. This indicates that the modified formulation of f does not offer any real advantage in solution quality. For this reason, the standard formulation will continue to be adopted in the remainder of the study (see Equation 5.2).

Trial	$\boldsymbol{\alpha}$	$\boldsymbol{\beta}$	**el**	**dt**	**e**	**Min**	**Aver**
T1ff	4	1	0.999	3	0.1	4.40E + 04	5.64E + 04
T2ff	4	1	0.999	3	0.1	4.91E + 04	5.58E + 04
T3ff	4	1	0.999	3	0.1	4.95E + 04	5.75E + 04
T4ff	4	1	0.999	3	0.1	4.89E + 04	5.73E + 04
T5ff	4	1	0.999	3	0.1	4.87E + 04	5.63E + 04
Average						4.80E + 04	5.67E + 04

Table 5.8: Case f_{var}: analysis with $dt = 3$

5.4 dt increase

Building on the insight that increasing the parameter dt tends to produce better results, we applied this adjustment to the standard configuration. The outcomes obtained under these conditions (Table 5.9) are slightly better than those of the reference case (Table 5.5), with only a negligible increase in minimum values and a decrease in average values. Although these differences are not substantial, they nonetheless confirm that a higher pheromone deposit can enhance the algorithm's ability to reinforce promising solutions, even when the standard cost formulation is used. A fascinating behaviour emerged when examining the number of cells whose pheromone level reached at least 10% of the maximum value in each row. In the initial iterations, the configuration with $dt = 4.5$ exhibited significantly fewer

cells above this threshold (Table B.5), indicating a more concentrated and decisive exploration pattern. However, by the end of the optimisation cycle, the number of such cells is comparable to those observed in the case with $dt = 0.05$ (Table B.1), previously discussed in Section 5.2.2. This could explain the result: a higher initial pheromone level can immediately direct the algorithm towards solutions with good results, but also prevent the exploration of initially less efficient solutions. So the solutions are better on average (the average ΔV decreases), but initially less promising solutions can subsequently yield lower ΔV. The fact that the number of final cells remains similar indicates a general balance in the algorithm.

Trial	$\boldsymbol{\alpha}$	$\boldsymbol{\beta}$	**el**	**dt**	**e**	**Min**	**Aver**
T1t	4	1	0.999	4.5	0.1	4.96E + 04	5.41E + 04
T2t	4	1	0.999	4.5	0.1	5.18E + 04	5.41E + 04
T3t	4	1	0.999	4.5	0.1	5.11E + 04	5.60E + 04
T4t	4	1	0.999	4.5	0.1	5.00E + 04	5.26E + 04
T5t	4	1	0.999	4.5	0.1	4.81E + 04	5.15E + 04
T6t	4	1	0.999	4.5	0.1	4.80E + 04	5.23E + 04
T7t	4	1	0.999	4.5	0.1	5.05E + 04	5.48E + 04
T8t	4	1	0.999	4.5	0.1	5.21E + 04	5.75E + 04
T9t	4	1	0.999	4.5	0.1	5.05E + 04	5.41E + 04
T10t	4	1	0.999	4.5	0.1	4.96E + 04	5.38E + 04
Average						5.02E + 04	5.41E + 04

Table 5.9: Case B4.9: analysis with $dt = 4.5$

5.5 Variable alpha

The parameter α plays a crucial role within the algorithm, as it determines the relative weight assigned to the heuristic information in the transition rule (Equation 4.1). By increasing its value, the behaviour of the artificial ants becomes progressively more greedy: the decisions tend to rely increasingly on the local heuristic, typically represented by the inverse of the distance in classical TSP formulations, while the relative influence of the pheromone trail diminishes. As a consequence, higher values of α naturally push the algorithm toward a less exploratory and more exploitative search regime.

Despite this intrinsic risk, adopting a stronger emphasis on the heuristic can be advantageous in the class of problems considered here, which in essence corresponds to a TSP. In this context, the heuristic information (in our specific case, the transfer cost between one debris and another) is highly informative and strongly

correlated with the actual quality of the solution. When the heuristic is reliable, steering the search process to exploit it more aggressively can significantly accelerate convergence and guide the ants toward promising regions of the solution space.
Nevertheless, relying too heavily on the heuristic from the outset may lead to premature convergence, with the colony focusing too early on a limited subset of routes and consequently losing diversity. To mitigate this risk, a variable and progressive approach was adopted for the parameter α, allowing its value to evolve dynamically during the optimisation process. Specifically, the parameter is updated at each iteration, starting from an initial value $\alpha_{in} = 4$ and gradually rising to a final value $\alpha_{fin} = 6$, according to the linear schedule:

$$\alpha = 4 + 2\frac{i}{miter} \tag{5.3}$$

where *miter* denotes the total number of iterations and i represents the current iteration index. This smooth increase ensures that, in the early phases of the algorithm, the ants benefit from more exploratory behaviour. In contrast, in later iterations, the algorithm transitions to a more focused, exploitative phase. Such a strategy proved particularly effective at balancing exploration and exploitation, especially given the relatively high amount of pheromone deposited per iteration, which further stabilises convergence in the later stages.
The results obtained clearly confirm the effectiveness of this adaptive strategy. Not only does the algorithm manage to reach the lowest absolute minimum value of ΔV recorded among all tested configurations, but it also achieves, for the first time, a mean ΔV lower than 5.00E + 04 m/s. This outcome highlights both the robustness of the approach and its ability to exploit the problem's structure.

Trial	$\boldsymbol{\alpha_{in}}$	$\boldsymbol{\alpha_{fin}}$	$\boldsymbol{\beta}$	**el**	**dt**	**e**	**Min**	**Aver**
T1a	4	6	1	0.999	4.5	0.1	4.92E + 04	5.06E + 04
T2a	4	6	1	0.999	4.5	0.1	5.02E + 04	5.23E + 04
T3a	4	6	1	0.999	4.5	0.1	4.87E + 04	5.24E + 04
T4a	4	6	1	0.999	4.5	0.1	4.19E + 04	5.21E + 04
T5a	4	6	1	0.999	4.5	0.1	4.61E + 04	5.02E + 04
T6a	4	6	1	0.999	4.5	0.1	5.07E + 04	5.28E + 04
T7a	4	6	1	0.999	4.5	0.1	4.74E + 04	5.33E + 04
T8a	4	6	1	0.999	4.5	0.1	4.72E + 04	5.30E + 04
T9a	4	6	1	0.999	4.5	0.1	4.80E + 04	4.98E + 04
T10a	4	6	1	0.999	4.5	0.1	4.87E + 04	5.05E + 04
Average							4.78E + 04	5.17E + 04

Table 5.10: Case B4.9: analysis with α variable

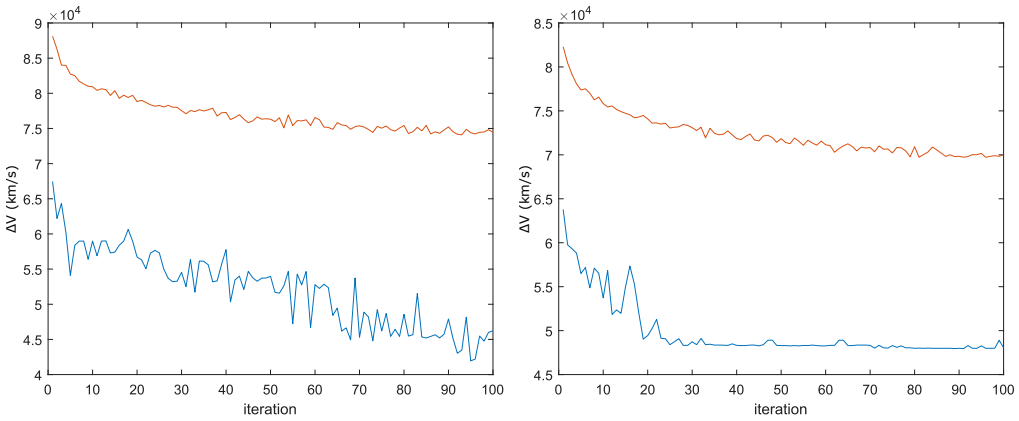

(a) Trial T4a: best minimun **(b)** Trial T9a: best average

Figure 5.6: α variable: best minimum and average

Comparing the best trials, specifically, **T4a** for the minimum value and **T9a** for the best average performance, two clearly distinct behaviours emerge, each reflecting a different balance between exploration and exploitation within the colony's dynamics. In the first case (T4a), the trend of the minimum ΔV values shows a markedly irregular pattern, characterised by numerous oscillations and sudden improvements. Such fluctuations indicate a persistently exploratory search, where the ants continue sampling alternative paths throughout the optimisation process rather than prematurely converging on a single dominant route. This ongoing diversity allows the algorithm to keep discovering new, sometimes better solutions, even in the later stages, leading to the achievement of the global minimum only in the final ten iterations. By contrast, the behaviour observed in T9a is notably more stable. The minimum ΔV is reached relatively early, between the twentieth and thirtieth iterations, and remains essentially unchanged for the remainder of the process. The curve shows limited variability, reflecting a rapid consolidation around a specific set of routes. While this early stabilisation yields an excellent average performance, as the solutions generated over time are consistently close to the best found, it comes at the cost of a less competitive absolute minimum. The algorithm becomes efficient but not exploratory: it quickly commits to a promising region of the solution space, but this limits its ability to discover deeper minima later.
When a reasonably good but suboptimal solution is found too early, the pheromone deposited on its edges biases subsequent ants toward repeatedly selecting that same solution. As iterations progress, the accumulated pheromone becomes increasingly dominant, making it progressively harder for the colony to escape from this attractor state and explore alternative, potentially superior trajectories. Consequently, the algorithm exhibits excellent stability but reduced adaptability, which explains the contrast between T9a's superior average and T4a's superior absolute minimum.

5.6 Iterations increase

All previous analyses maintained a similar computational cost, with a simulation duration of $3 \div 7$ minutes, mainly because the total number of iterations *miter* was set to 100. In this last phase of the study, all parameters were kept constant except *miter*, which was set to 1000 and 5000 in two simulation sets. The results obtained must be commented on in comparison to the computational cost of acquiring them: in fact, with 1000 iterations, the duration of the individual trials falls within the range $30 \div 60$ minutes, while with 5000 iterations, the duration increases to $150 \div 300$ minutes. The best case with 1000 iterations (**T7i**) shows a slight decrease in the minimums and a significant decrease in the averages compared to the case analysed previously. In this case too, the algorithm falls into a local minimum fairly quickly, before the hundredth iteration, and remains constant for the rest of the iterations. For this reason, the calculation of the minimum ΔV's averages is better than in the previous case. This "distorted" result can still be considered a starting point for subsequent parameter optimisation with a higher number of iterations, all within a simulation duration that remains manageable. The case with 5000 iterations can be immediately discarded because, given the excessive duration of each iteration, it shows a slight increase in the minima and a slight decrease in the averages compared to the study with 1000 iterations, which does not justify the increase in computational cost. Looking at the trend of the trial with the best result (**T2ii**), it is not convincing, as it immediately enters a local minimum and remains approximately constant throughout the simulation, also presenting strong oscillations that increase its cost.

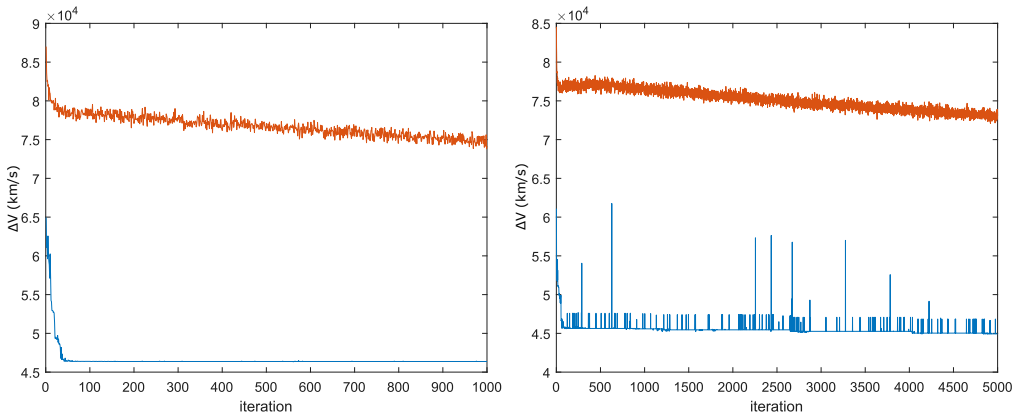

(a) Trial T7i **(b)** Trial T2ii

Figure 5.7: *miter* = 1000/5000: best averages

Trial	$\boldsymbol{\alpha_{in}}$	$\boldsymbol{\alpha_{fin}}$	$\boldsymbol{\beta}$	**el**	**dt**	**e**	**Min**	**Aver**
T1i	4	6	1	0.999	4.5	0.1	4.60E + 04	4.72E + 04
T2i	4	6	1	0.999	4.5	0.1	4.56E + 04	5.05E + 04
T3i	4	6	1	0.999	4.5	0.1	4.66E + 04	4.77E + 04
T4i	4	6	1	0.999	4.5	0.1	4.87E + 04	5.05E + 04
T5i	4	6	1	0.999	4.5	0.1	4.72E + 04	5.10E + 04
T6i	4	6	1	0.999	4.5	0.1	4.80E + 04	5.14E + 04
T7i	4	6	1	0.999	4.5	0.1	4.63E + 04	4.66E + 04
T8i	4	6	1	0.999	4.5	0.1	4.71E + 04	5.18E + 04
T9i	4	6	1	0.999	4.5	0.1	4.72E + 04	4.96E + 04
T10i	4	6	1	0.999	4.5	0.1	4.87E + 04	4.94E + 04
Average							4.71E + 04	4.96E + 04

Table 5.11: Case B4.9: analysis with 1000 iterations

Trial	$\boldsymbol{\alpha_{in}}$	$\boldsymbol{\alpha_{fin}}$	$\boldsymbol{\beta}$	**el**	**dt**	**e**	**Min**	**Aver**
T1ii	4	6	1	0.999	4.5	0.1	4.82E + 04	4.90E + 04
T2ii	4	6	1	0.999	4.5	0.1	4.49E + 04	4.55E + 04
T3ii	4	6	1	0.999	4.5	0.1	4.91E + 04	4.99E + 04
T4ii	4	6	1	0.999	4.5	0.1	4.63E + 04	4.77E + 04
T5ii	4	6	1	0.999	4.5	0.1	4.78E + 04	4.98E + 04
T6ii	4	6	1	0.999	4.5	0.1	4.82E + 04	4.90E + 04
T7ii	4	6	1	0.999	4.5	0.1	4.49E + 04	4.55E + 04
T8ii	4	6	1	0.999	4.5	0.1	4.91E + 04	4.99E + 04
T9ii	4	6	1	0.999	4.5	0.1	4.91E + 04	5.04E + 04
T10ii	4	6	1	0.999	4.5	0.1	4.82E + 04	4.90E + 04
Average							4.76E + 04	4.86E + 04

Table 5.12: Case B4.9: analysis with 5000 iterations

Chapter 6

Conclusions

The issue of space debris is a serious concern that mandates targeted, worldwide action, not only policies to reduce debris generation from future missions but also ADR missions to eliminate the most hazardous debris from orbit. The purpose of this thesis is specifically to examine an ADR mission and its optimisation in terms of ΔV, using an ACO algorithm. The analysed problem involves a mission consisting of 123 debris pieces, introduced by GTOC9, referencing the winning solution of the JPL.
The thesis consisted of an analysis of the algorithm with a study of the effect of the main parameters, in order:

- preliminary study;
- effect of the ants' number;
- study of the pheromone matrix;
- effect of the variation in the calculation of the cost parameter f;
- effect of the increase in pheromone deposition;
- effect of the variation of the parameter α;
- effect of the increase in the number of iterations.

Overall, there was a significant improvement in the results, moving from the initial values with a $\Delta V = 5.50 \div 6.00\text{E}+04$ m/s to the best result of $\Delta V_{min} = 4.19\text{E}+04$ m/s. However, this is still far from the result of the winning solution of $\Delta V_{JPL} = 2.5326\text{E}+04$ m/s. This is probably due to the model's simplifications, such as the cost matrix, which considers only 5-day time slots.
Future analyses could focus on optimising the models and possibly combining ACO with other algorithms, such as genetic algorithms.

Appendix A

Debris orbital elements

Below is the debris database on which GTOC9 is based.

id	ref epoch [mjd2000]	a [m]	e	i [rad]	Ω [rad]	ω [rad]	M [rad]
000	2.194765E+04	7.165740E+06	1.487229E-03	1.708495	5.425149	0.518965	3.220888
001	2.216722E+04	7.119482E+06	1.681883E-02	1.719032	4.030232	2.249735	4.880728
002	2.197181E+04	7.159621E+06	3.792826E-03	1.695100	2.928707	4.493324	6.243761
003	2.216954E+04	7.110511E+06	6.666299E-03	1.694290	0.623365	3.411909	4.771420
004	2.205222E+04	7.102000E+06	1.829616E-03	1.749873	2.622564	2.397072	3.132921
005	2.197498E+04	7.173465E+06	8.500730E-03	1.725002	4.716882	2.987324	5.494481
006	2.214809E+04	7.058042E+06	8.723435E-03	1.720674	3.574643	4.981435	4.195619
007	2.214282E+04	7.059602E+06	2.493245E-03	1.706914	1.455986	4.302093	5.348153
008	2.212872E+04	7.134324E+06	1.627160E-02	1.744527	0.132978	5.838210	5.562178
009	2.203756E+04	7.147208E+06	8.007723E-03	1.705436	3.378731	1.276019	5.223427
010	2.218776E+04	7.162215E+06	2.402291E-03	1.717952	2.604417	1.894280	4.384844
011	2.209199E+04	7.232508E+06	1.177358E-03	1.706631	3.051655	1.707654	3.357483
012	2.192872E+04	7.158643E+06	1.004019E-02	1.732026	0.721701	2.945439	3.283550
013	2.217843E+04	7.236494E+06	3.312351E-03	1.713750	1.804366	4.148072	2.258170
014	2.213443E+04	7.183439E+06	5.811605E-03	1.698376	1.304970	4.990687	3.556253
015	2.205792E+04	7.182861E+06	7.267772E-03	1.725351	1.203530	5.517631	4.051394
016	2.202907E+04	7.089469E+06	8.932669E-03	1.715224	1.230442	2.912518	1.400851
017	2.197656E+04	7.172023E+06	7.589348E-03	1.712397	4.123162	2.723573	1.169763
018	2.197569E+04	7.116054E+06	8.945916E-03	1.720187	1.827976	0.910803	3.299909
019	2.193159E+04	7.130316E+06	1.101317E-02	1.721377	2.419138	2.102604	1.030948
020	2.195681E+04	7.012358E+06	3.730638E-03	1.714565	4.767906	2.224211	1.440759
021	2.207550E+04	7.059521E+06	5.303572E-03	1.721274	3.273719	3.328680	3.535566
022	2.206934E+04	7.062555E+06	4.344287E-03	1.727481	5.774706	5.532209	5.910383
023	2.194874E+04	7.157398E+06	1.521215E-02	1.721654	5.636359	2.610833	2.827198
024	2.202925E+04	7.155533E+06	1.332144E-02	1.717436	4.052507	0.724032	5.575959
025	2.213024E+04	7.146484E+06	8.869012E-03	1.715996	3.114967	4.910124	1.909932
026	2.206129E+04	7.103926E+06	5.856909E-03	1.695149	3.412728	3.545619	0.056164
027	2.203179E+04	7.179069E+06	1.246636E-02	1.727242	6.003371	4.248960	0.313089
028	2.210650E+04	7.154893E+06	8.590128E-03	1.712096	2.457221	0.432171	4.343796
029	2.197933E+04	7.212281E+06	5.395627E-03	1.724272	5.039544	5.122513	0.012920
030	2.217195E+04	7.043105E+06	6.449478E-03	1.713199	0.789655	5.559342	0.155340

id	ref epoch [mjd2000]	a [m]	e	i [rad]	Ω [rad]	ω [rad]	M [rad]
031	2.210095E+04	7.051174E+06	6.440428E-03	1.742004	5.446301	0.837217	2.310166
032	2.208747E+04	7.138316E+06	1.551066E-02	1.723685	2.359166	5.902230	5.819602
033	2.208937E+04	7.173333E+06	1.758879E-04	1.743863	5.394232	2.672470	3.919481
034	2.198351E+04	7.077974E+06	1.400994E-02	1.721533	1.182380	2.416966	3.348460
035	2.219032E+04	7.181534E+06	8.269410E-03	1.687254	4.195371	4.724818	1.982827
036	2.209062E+04	7.126644E+06	1.888474E-02	1.732088	4.636137	1.893613	1.964868
037	2.200913E+04	7.052246E+06	1.022611E-03	1.704517	5.605575	0.361641	5.343174
038	2.193169E+04	7.215644E+06	7.675381E-03	1.718896	0.735201	3.402516	4.706336
039	2.207348E+04	7.215587E+06	7.144785E-03	1.742835	1.206743	1.158549	2.909120
040	2.210660E+04	7.115545E+06	3.482280E-03	1.717730	3.341408	5.494110	0.556703
041	2.218155E+04	7.053731E+06	3.786224E-03	1.703549	2.847406	3.660832	3.818279
042	2.207236E+04	7.160058E+06	5.817049E-03	1.722287	0.249414	2.496451	5.814079
043	2.207235E+04	7.056234E+06	8.318607E-03	1.724840	2.772746	5.473028	5.664093
044	2.205522E+04	7.228525E+06	1.643274E-03	1.742501	5.789705	4.709001	6.272825
045	2.197094E+04	7.196788E+06	8.962027E-03	1.713106	5.716823	0.993884	5.286049
046	2.204423E+04	7.172848E+06	7.915919E-04	1.733290	5.839741	1.283464	0.563965
047	2.211653E+04	7.198381E+06	7.011095E-04	1.703918	3.655643	3.575376	0.199537
048	2.215519E+04	7.226075E+06	3.207868E-03	1.704059	3.988191	3.381501	3.558539
049	2.191926E+04	7.163630E+06	6.002220E-03	1.694043	0.288962	1.066419	4.403553
050	2.218266E+04	7.229884E+06	2.991762E-03	1.713430	5.692620	1.223314	0.041319
051	2.204492E+04	7.273982E+06	4.550194E-04	1.698442	6.069515	2.512675	0.408602
052	2.207336E+04	7.184065E+06	1.220089E-02	1.703238	4.387526	4.285731	2.264961
053	2.220521E+04	7.120605E+06	1.874848E-02	1.724352	1.194044	6.033829	2.318075
054	2.217881E+04	7.082709E+06	5.462430E-03	1.726013	0.765129	3.875106	4.174192
055	2.191914E+04	7.111954E+06	7.219400E-03	1.700845	2.228756	3.020463	0.246080
056	2.216654E+04	7.132885E+06	1.571059E-02	1.721805	1.399217	2.812724	2.125569
057	2.217847E+04	7.114376E+06	3.042113E-04	1.693049	1.519339	1.559974	0.568255
058	2.200633E+04	7.105628E+06	1.173294E-02	1.726230	3.144176	5.261153	2.566383
059	2.216324E+04	7.271247E+06	3.762196E-04	1.721280	0.483958	2.216004	5.077246
060	2.219332E+04	7.081623E+06	1.083219E-02	1.710420	3.606112	3.424865	0.752168
061	2.218710E+04	7.147664E+06	9.661350E-03	1.715856	5.141398	3.776268	4.228404
062	2.212612E+04	7.075266E+06	1.008533E-02	1.727056	3.735921	1.948972	5.167473
063	2.210983E+04	7.077483E+06	8.976180E-03	1.714842	2.315854	5.264361	2.634042
064	2.194917E+04	7.108669E+06	7.197755E-03	1.720662	1.172257	3.004086	1.391617
065	2.211224E+04	7.062977E+06	8.469514E-03	1.726143	5.705315	5.644936	2.911421
066	2.200553E+04	7.209849E+06	4.406078E-03	1.716267	5.888406	3.173530	3.087900
067	2.214051E+04	7.079321E+06	7.897700E-03	1.720888	1.951326	1.878163	4.973612
068	2.218606E+04	7.225611E+06	1.515064E-03	1.736646	0.585338	5.490014	2.043859
069	2.215369E+04	7.186116E+06	1.241328E-02	1.722031	4.293977	3.331646	1.942062
070	2.200810E+04	7.064874E+06	7.411795E-03	1.708306	5.131597	1.404040	0.665708
071	2.205165E+04	7.096803E+06	7.960407E-03	1.719398	0.621217	2.591944	1.262710
072	2.203721E+04	7.105028E+06	9.061772E-03	1.714198	4.331261	0.760018	2.806373
073	2.211784E+04	7.145101E+06	9.377102E-03	1.719102	5.802520	3.727008	3.417270
074	2.205441E+04	7.177235E+06	1.066132E-02	1.725437	1.056123	2.359200	2.830144
075	2.204904E+04	7.197173E+06	6.928016E-03	1.713287	3.702908	5.880496	5.617193
076	2.219879E+04	7.179588E+06	6.961320E-03	1.723178	3.986177	2.323052	2.741086
077	2.216447E+04	7.183267E+06	5.802932E-03	1.703986	4.429211	3.186347	3.465833
078	2.202127E+04	7.155297E+06	8.919285E-03	1.716830	5.381843	2.576198	5.672909
079	2.199625E+04	7.159032E+06	9.545917E-03	1.720734	4.277214	3.308775	0.438950
080	2.212003E+04	7.192667E+06	7.196392E-03	1.714367	2.971374	2.529460	2.902169

id	ref epoch [mjd2000]	a [m]	e	i [rad]	Ω [rad]	ω [rad]	M [rad]
081	2.216712E+04	7.090426E+06	8.276434E-03	1.722901	1.372865	4.590202	3.573541
082	2.194422E+04	7.083098E+06	7.863101E-03	1.729562	2.464774	3.146138	2.038284
083	2.206312E+04	7.180496E+06	1.016109E-02	1.714223	5.963142	0.939159	4.733134
084	2.204872E+04	7.121908E+06	8.197778E-03	1.709435	3.457047	5.612360	1.346153
085	2.206968E+04	7.116671E+06	6.537924E-03	1.708913	5.258345	3.309209	3.786573
086	2.219321E+04	7.152739E+06	9.951398E-03	1.715439	2.187336	2.511077	5.954173
087	2.205428E+04	7.190591E+06	1.061142E-02	1.722450	5.987323	5.062871	0.708278
088	2.217254E+04	7.140781E+06	7.147995E-03	1.720308	0.338059	2.985778	3.030568
089	2.201389E+04	7.093749E+06	9.108163E-03	1.718258	4.175792	4.128416	2.650922
090	2.211841E+04	7.071213E+06	1.054442E-02	1.719101	3.258468	5.719657	2.314301
091	2.208636E+04	7.177201E+06	1.220831E-02	1.728021	1.746973	3.930427	4.515732
092	2.218435E+04	7.187982E+06	9.506758E-03	1.717506	2.689546	2.259179	5.786908
093	2.214980E+04	7.168720E+06	7.413429E-03	1.723043	0.842468	5.150263	2.479731
094	2.217420E+04	7.194506E+06	7.911788E-03	1.728822	4.356642	3.408965	0.714002
095	2.218765E+04	7.118953E+06	8.912625E-03	1.718105	5.204496	4.868493	3.383712
096	2.203099E+04	7.206845E+06	4.479566E-03	1.708563	2.109035	2.904670	1.948625
097	2.211949E+04	7.100308E+06	1.035084E-02	1.719615	3.689100	0.832821	3.773218
098	2.194909E+04	7.082544E+06	6.804366E-03	1.726836	4.591515	5.623187	1.634959
099	2.202884E+04	7.118139E+06	9.089484E-03	1.707249	3.095810	3.927277	4.964431
100	2.205307E+04	7.181787E+06	6.312353E-03	1.713634	0.511989	4.543944	2.792506
101	2.218622E+04	7.147865E+06	8.013998E-03	1.715914	1.091129	3.200268	4.177828
102	2.200123E+04	7.185711E+06	8.484774E-03	1.718214	3.510863	1.270780	3.478536
103	2.210288E+04	7.179415E+06	6.077320E-03	1.726014	5.585424	4.823272	5.987073
104	2.217170E+04	7.196931E+06	7.272520E-03	1.723218	2.241528	5.478134	2.330169
105	2.198502E+04	7.093851E+06	8.825184E-03	1.720579	1.740478	3.153063	3.055332
106	2.216874E+04	7.089948E+06	8.300417E-03	1.727442	2.845349	2.888266	4.392190
107	2.206597E+04	7.129963E+06	1.020623E-02	1.723037	4.146741	4.465892	1.942110
108	2.202581E+04	7.134785E+06	8.639302E-03	1.721171	5.606430	0.945518	3.702861
109	2.211607E+04	7.179177E+06	7.457318E-03	1.712947	0.608114	5.865917	5.043250
110	2.214238E+04	7.194036E+06	7.241760E-03	1.713933	3.242067	2.207023	3.986509
111	2.205789E+04	7.144598E+06	8.247996E-03	1.727633	0.174149	4.713084	5.240113
112	2.201282E+04	7.166929E+06	9.163716E-03	1.717183	1.317390	0.496302	4.810755
113	2.218802E+04	7.195201E+06	9.672445E-03	1.715879	2.650767	3.611016	5.662998
114	2.219543E+04	7.160463E+06	8.470122E-03	1.724048	3.309752	1.021305	3.179685
115	2.204427E+04	7.111386E+06	8.892067E-03	1.708108	5.703144	3.898746	0.796452
116	2.198627E+04	7.082062E+06	9.068070E-03	1.720259	0.986342	4.316990	2.413576
117	2.193877E+04	7.097555E+06	1.016760E-02	1.718472	3.777684	5.422604	3.878428
118	2.199532E+04	7.122637E+06	7.791942E-03	1.712661	2.010958	2.149133	5.130983
119	2.207119E+04	7.103559E+06	8.924013E-03	1.724654	1.075671	5.036497	2.572293
120	2.211991E+04	7.097439E+06	9.290977E-03	1.716961	4.924793	3.572165	0.918947
121	2.218281E+04	7.146086E+06	8.277566E-03	1.720248	5.498603	2.385792	4.007520
122	2.203813E+04	7.168956E+06	8.964147E-03	1.718743	2.853116	4.211586	5.572831

Appendix B

Pheromones matrix

To avoid overloading the discussion, the tables containing the pheromone cells are shown below.

Case B4.9	Iteration																		
	1	2	3	4	5	6	7	8	9	10	20	30	40	50	60	70	80	90	100
T1	13786	12461	10602	7192	3248	2062	853	542	486	426	329	309	282	301	294	299	280	283	305
T2	13054	8930	4945	2739	1134	781	762	622	632	529	493	490	473	476	462	477	473	492	511
T3	10770	9860	7821	4479	2698	1446	1160	911	782	697	330	293	284	298	289	274	266	287	290
T4	12848	8961	3906	2171	1173	1099	808	655	603	524	440	441	412	415	426	435	430	442	462
T5	13180	9667	4972	1689	898	742	652	605	584	584	443	421	422	439	434	452	445	442	439
T6	12324	10029	5413	3539	2381	1194	788	483	454	450	367	351	357	366	368	364	391	398	399
T7	13192	10179	6980	3498	2150	1006	608	550	444	431	357	354	351	351	358	348	354	372	389
T8	13420	10885	5639	2555	1002	651	437	394	383	376	368	358	350	369	379	379	362	353	345
T9	13908	12813	10281	7774	4601	2598	1115	801	596	453	359	319	306	302	298	302	305	316	314
T10	12402	8748	5478	3809	2246	1429	1228	690	540	515	426	438	440	417	416	419	417	394	399
Average	12888.4	10253.3	6603.7	3944.5	2153.1	1300.8	841.1	625.3	550.4	498.5	391.2	377.4	367.7	373.4	372.4	374.9	372.3	377.9	385.3

Table B.1: Case B4.9: t1k analysis, number of 10% cells

$e = 0.01$	Iteration																		
	1	2	3	4	5	6	7	8	9	10	20	30	40	50	60	70	80	90	100
T1b	10773	9700	8410	6778	5056	3886	3011	2491	1721	1337	372	351	347	348	352	351	346	354	349
T2b	12856	10130	5763	4383	3311	2403	1529	1011	807	599	521	531	532	536	541	529	518	519	516
T3b	13180	10051	6929	3808	2609	1690	1054	676	635	625	509	493	501	496	522	523	522	529	534
T4b	12325	10992	7363	5462	3198	1778	1437	828	769	561	471	452	456	450	443	440	449	452	445
T5b	13195	10894	6664	3936	2353	1360	1129	892	752	731	472	453	444	456	460	472	468	477	479
Average	12465.8	10353.4	7025.8	4873.4	3305.4	2223.4	1632	1179.6	936.8	770.6	469	456	456	457.2	463.6	463	460.6	466.2	464.6

Table B.2: Case B4.9 ($e = 0.01$): t1k analysis, number of 10% cells

$f_{var},\ dt = 1.5$	Iteration																		
	1	2	3	4	5	6	7	8	9	10	20	30	40	50	60	70	80	90	100
T1f	15006	15006	15006	15006	15006	15006	15006	15006	15006	15006	15006	15006	15006	12596	2964	512	399	387	371
T2f	15006	15006	15006	15006	15006	15006	15006	15006	15006	15006	15006	15006	15006	14774	6224	998	430	380	358
T3f	15006	15006	15006	15006	15006	15006	15006	15006	15006	15006	15006	15006	15006	11992	4428	796	541	442	442
T4f	15006	15006	15006	15006	15006	15006	15006	15006	15006	15006	15006	15006	15006	14546	5566	757	395	377	347
T5f	15006	15006	15006	15006	15006	15006	15006	15006	15006	15006	15006	15006	15006	13675	4645	634	417	375	358
Average	15006	15006	15006	15006	15006	15006	15006	15006	15006	15006	15006	15006	15006	13516.6	4765.4	739.4	436.4	392.2	375.2
T6f	15006	15006	15006	15006	15006	15006	15006	15006	15006	15006	15006	15006	15006	15006	15006	15006	15006	15006	15006
T7f	15006	15006	15006	15006	15006	15006	15006	15006	15006	15006	15006	15006	15006	15006	15006	15006	15006	15006	15006
T8f	15006	15006	15006	15006	15006	15006	15006	15006	15006	15006	15006	15006	15006	15006	15006	15006	15006	15006	15006
T9f	15006	15006	15006	15006	15006	15006	15006	15006	15006	15006	15006	15006	15006	15006	15006	15006	15006	15006	15006
T10f	15006	15006	15006	15006	15006	15006	15006	15006	15006	15006	15006	15006	15006	15006	15006	15006	15006	15006	15006
Average	15006	15006	15006	15006	15006	15006	15006	15006	15006	15006	15006	15006	15006	15006	15006	15006	15006	15006	15006

Table B.3: Case f_{var} $(dt = 1.5)$: t1k analysis, number of 10% cells

$f_{var},\ dt = 3$	Iteration																		
	1	2	3	4	5	6	7	8	9	10	20	30	40	50	60	70	80	90	100
T1ff	15006	15006	15006	15006	15006	15006	15006	15006	15006	15006	15006	15006	13761	5361	756	500	404	406	385
T2ff	15006	15006	15006	15006	15006	15006	15006	15006	15006	15006	15006	15006	14664	6707	821	476	434	390	356
T3ff	15006	15006	15006	15006	15006	15006	15006	15006	15006	15006	15006	15006	14891	9255	2492	476	385	350	329
T4ff	15006	15006	15006	15006	15006	15006	15006	15006	15006	15006	15006	15006	14327	5938	1239	548	477	445	431
T5ff	15006	15006	15006	15006	15006	15006	15006	15006	15006	15006	15006	15006	14658	8942	1103	438	385	369	357
Average	15006	15006	15006	15006	15006	15006	15006	15006	15006	15006	15006	15006	14460.2	7240.6	1282.2	487.6	417	392	371.6

Table B.4: Case f_{var} $(dt = 3)$ t1k analysis, number of 10% cells

$dt = 4.5$	Iteration																			
	1	2	3	4	5	6	7	8	9	10	20	30	40	50	60	70	80	90	100
T1t	963	665	542	474	421	429	443	445	456	443	440	460	483	464	433	435	451	454	457
T2t	916	530	422	372	333	321	334	330	323	318	324	364	376	377	381	377	370	379	383
T3t	767	567	509	451	412	400	377	384	375	375	373	377	366	359	348	322	338	340	346
T4t	748	498	434	385	344	338	333	333	318	311	312	301	302	309	300	313	314	313	307
T5t	826	562	457	416	374	373	364	366	372	361	334	352	350	374	388	399	395	397	398
T6t	749	504	458	448	411	409	404	399	381	366	354	339	340	349	345	349	329	341	337
T7t	1029	695	510	493	474	446	432	406	410	418	418	413	401	405	430	436	458	477	477
T8t	830	583	526	516	495	475	476	467	464	458	393	377	340	343	324	316	339	349	360
T9t	829	619	527	497	450	433	433	399	387	364	343	348	351	347	356	352	349	350	344
T10t	811	532	450	435	416	407	403	408	405	406	379	356	359	359	375	387	389	379	373
Average	846.8	575.5	483.5	448.7	413	403.1	399.9	393.7	389.1	382	367	368.7	366.8	368.6	368	368.6	373.2	377.9	378.2

Table B.5: Case B4.9 ($dt = 4.5$): t1k analysis, number of 10% cells

$\alpha = 4 \div 6$	Iteration																		
	1	2	3	4	5	6	7	8	9	10	20	30	40	50	60	70	80	90	100
T1a	874	475	408	350	327	323	302	310	316	319	325	331	330	333	327	322	325	320	321
T2a	881	632	578	554	520	508	482	427	442	447	491	486	492	511	516	513	471	484	477
T3a	764	586	472	451	400	377	372	376	374	371	350	338	348	365	376	371	377	372	370
T4a	588	480	408	371	353	341	327	323	321	321	300	301	294	300	301	309	300	297	293
T5a	899	630	450	418	403	376	396	389	393	387	445	458	458	475	472	486	490	482	478
T6a	855	589	534	508	488	426	425	415	409	412	396	411	381	375	367	367	348	347	333
T7a	884	494	451	390	362	343	325	325	323	327	297	298	317	300	299	291	309	311	321
T8a	887	646	573	525	472	441	439	399	385	394	399	398	386	415	419	413	404	421	417
T9a	711	504	413	392	365	353	355	364	356	344	328	341	353	354	346	342	345	337	336
T10a	767	575	481	439	420	399	396	395	392	395	356	351	342	339	340	334	333	333	330
Average	811	561.1	476.8	439.8	411	388.7	381.9	372.3	371.1	371.7	368.7	371.3	370.1	376.7	376.3	374.8	370.2	370.4	367.6

Table B.6: Case B4.9 (α variable): t1k analysis, number of 10% cells

1000 iter	Iteration																		
	1	2	3	4	5	6	7	8	9	10	200	300	400	500	600	700	800	900	1000
T1i	588	447	377	342	325	327	309	317	299	282	280	277	276	268	268	267	267	267	261
T2i	912	617	512	475	454	460	420	407	381	338	346	324	331	317	320	323	326	328	327
T3i	791	507	409	380	351	342	350	355	362	319	317	312	313	314	313	312	311	301	316
T4i	878	510	422	352	344	331	321	304	298	306	289	289	281	283	290	294	284	286	276
T5i	864	628	497	460	409	405	377	381	390	370	374	373	363	353	363	367	344	354	344
T6i	1015	706	594	547	536	532	534	532	535	455	464	450	437	444	430	440	431	398	428
T7i	840	603	544	487	483	488	478	447	444	384	379	381	373	375	377	373	369	367	361
T8i	773	520	456	397	362	342	322	312	310	340	321	314	308	309	309	307	306	319	312
T9i	827	592	527	461	450	454	452	454	451	434	422	414	422	386	414	415	416	415	422
T10i	944	647	467	426	395	384	375	375	395	448	413	413	417	418	414	415	421	415	418
Average	843.2	577.7	480.5	432.7	410.9	406.5	393.8	388.4	386.5	367.6	360.5	354.7	352.1	346.7	349.8	351.3	347.5	345	346.5

Table B.7: Case B4.9 (1000 iterations): t1k analysis, number of 10% cells

5000 iter	Iteration																		
	1	2	3	4	5	6	7	8	9	10	1000	1500	2000	2500	3000	3500	4000	4500	5000
T1ii	588	444	381	338	296	276	272	280	284	282	286	273	278	275	260	270	269	268	265
T2ii	802	558	503	467	445	427	413	408	400	397	291	290	289	291	288	286	282	280	276
T3ii	719	494	407	384	332	320	323	315	304	309	266	271	264	263	263	258	264	261	263
T4ii	868	567	451	439	427	396	379	383	378	376	378	392	379	377	386	382	379	378	383
T5ii	892	590	592	514	452	472	463	445	432	442	428	415	436	432	425	406	387	333	418
T6ii	588	444	381	338	296	276	272	280	284	287	265	261	257	260	257	260	255	254	254
T7ii	802	558	503	467	445	427	413	408	400	397	291	290	289	291	288	286	282	280	276
T8ii	719	494	407	384	332	320	323	315	304	309	266	271	264	263	263	258	264	261	263
T9ii	802	441	368	337	326	329	326	319	320	300	259	257	255	253	261	250	255	255	252
T10ii	588	444	381	338	296	276	272	280	284	287	265	261	257	260	257	260	255	254	254
Average	736.8	503.4	437.4	400.6	364.7	351.9	345.6	343.3	339	338.6	299.5	298.1	296.8	296.5	294.8	291.6	289.2	282.4	290.4

Table B.8: Case B4.9 (5000 iterations): t1k analysis, number of 10% cells

Bibliography

[1] NASA. *Astromaterials Research & Exploration Science*. URL: https://orbitaldebris.jsc.nasa.gov/faq/# (cit. on p. 1).

[2] INAF - Osservatorio Astronomico d'Abruzzo. *Space Debris Program*. URL: https://www.oa-abruzzo.inaf.it/progetti-databases/space-debris-program/ (cit. on p. 1).

[3] ESA. *Detriti spaziali: È crisi?* URL: https://www.esa.int/Space_in_Member_States/Italy/Detriti_spaziali_E_crisi (cit. on p. 2).

[4] Donald Kessler, Nicholas Johnson, J.-C Liou, and Mark Matney. «The Kessler Syndrome: Implications to Future Space operations». In: *Advances in the Astronautical Sciences* 137 (Jan. 2010) (cit. on pp. 2, 3).

[5] Loretta Hall. «The History of Space Debris». In: *Space Traffic Management Conference. 19* (2014) (cit. on p. 3).

[6] ESA. *Position Paper on Space Debris Mitigation: Implementing Zero Debris Creation Zones*. ESA SP-1301. 2004. URL: https://www.esa.int/esapub/sp/sp1301/sp1301.pdf (cit. on p. 3).

[7] National Research Council. *Orbital Debris: A Technical Assessment*. Washington, DC: The National Academies Press, 1995. URL: https://nap.nationalacademies.org/catalog/4765/orbital-debris-a-technical-assessment (cit. on p. 3).

[8] Nicholas Johnson, E. Stansbery, J.-C Liou, M. Horstman, Christopher Stokely, and D. Whitlock. «The characteristics and consequences of the break-up of the Fengyun-1C spacecraft». In: *Acta Astronautica* 63 (July 2008), pp. 128–135. DOI: 10.1016/j.actaastro.2007.12.044 (cit. on p. 4).

[9] ESA Space Debris Office. *ESA'S ANNUAL SPACE ENVIRONMENT REPORT*. GEN-DB-LOG-00288-OPS-SD. 2025 (cit. on pp. 5–7, 11).

[10] ESA & UNOOSA. *Space debris infographics and podcast*. URL: https://www.esa.int/Space_Safety/Space_Debris/ESA_UNOOSA_space_debris_infographics_and_podcast (cit. on p. 7).

[11] ESA. *ESA's Zero Debris approach*. URL: https://www.esa.int/Space_Safety/Clean_Space/ESA_s_Zero_Debris_approach (cit. on p. 8).

[12] Brent Barbee, Salvatore Alfano, Elfego Pinon, Kenn Gold, and David Gaylor. «Design of spacecraft missions to remove multiple orbital debris objects». In: vol. 144. Apr. 2011, pp. 1–14. DOI: 10.1109/AERO.2011.5747303 (cit. on p. 9).

[13] José P. Ferreira, Ziyu Huang, Ken-ichi Nomura, and Joseph Wang. «Potential Ozone Depletion From Satellite Demise During Atmospheric Reentry in the Era of Mega-Constellations». In: *Geophysical Research Letters* 51.11 (2024). DOI: https://doi.org/10.1029/2024GL109280. URL: https://agupubs.onlinelibrary.wiley.com/doi/abs/10.1029/2024GL109280 (cit. on p. 12).

[14] Bate Roger R. *Fundamentals of astrodynamics / Roger R. Bate, Donald D. Mueller, Jerry E. White*. eng. New York: Dover Publications, 1971. ISBN: 978-04-86600-61-1 (cit. on pp. 13, 14, 16, 20, 21).

[15] David A. Vallado and Wayne D. McClain. *Fundamentals of astrodynamics and applications / David A. Vallado ; with technical contrib. by Wayne D. McClain*. eng. 2nd ed. «The» space technology library. El Segundo Dordrecht: Microcosm Press Kluwer Academic Publ., 2001. ISBN: 0-7923-6903-3 (cit. on pp. 17, 20, 21, 23).

[16] Wikipedia. *Giorno giuliano*. URL: https://it.wikipedia.org/wiki/Giorno_giuliano (cit. on p. 23).

[17] D. Izzo and M. Maertens. «The Kessler Run: On the Design of the GTOC9 Challenge». In: *Acta Futura* 11 (Jan. 2018), pp. 11–24 (cit. on pp. 24, 26).

[18] Anastassios Petropoulos et al. «GTOC9: Methods and Results from the Jet Propulsion Laboratory Team». In: (May 2017) (cit. on pp. 24, 27, 28).

[19] Hong-Xin Shen and Lorenzo Casalino. «Simple ΔV Approximation for Optimization of Debris-to-Debris Transfers». In: *Journal of Spacecraft and Rockets* 58 (Dec. 2020), pp. 1–6. DOI: 10.2514/1.A34831 (cit. on pp. 28, 31).

[20] Daniele Poma. «Trajectory optimization with chemical propulsion for multiple debris removal missions». MA thesis. Politecnico di Torino, 2024 (cit. on pp. 28, 40, 41).

[21] Marco Dorigo and Thomas Stützle. *Ant Colony Optimization*. USA: Bradford Company, 2004. ISBN: 0262042193 (cit. on pp. 33–38).

[22] Kush Shrivastava and Dr Shishir Kumar. «The Effectiveness of Parameter Tuning on Ant Colony Optimization for Solving the Travelling Salesman Problem». In: Dec. 2019. DOI: 10.1109/CSNT.2018.17 (cit. on pp. 40, 41).